RC CIRCUIT MODEL-BASED ANOMALY DETECTION FOR LI-ION BATTERIES

by

Tunga R

APPROVED BY SUPERVISORY COMMITTEE:

Dr. Justin Ruths, Chair

Dr. Stephen Yurkovich

Dr. Babak Fahimi

Dr. Nicholas Gans

This thesis class file

is dedicated to my parents and my advisor,

who have been my constant support

RC CIRCUIT MODEL-BASED ANOMALY DETECTION FOR LI-ION BATTERIES

by

TUNGA R, BE

THESIS

Presented to the Faculty of

The University of Texas at Dallas

in Partial Fulfillment

of the Requirements

for the Degree of

MASTERS OF SCIENCE IN

ELECTRICAL ENGINEERING

THE UNIVERSITY OF TEXAS AT DALLAS

May 2018

ACKNOWLEDGMENTS

I am very thankful to my advisor, Dr. Justin Ruths who motivated and guided me throughout my research and my Masters in Electrical Engineering at the University of Texas at Dallas. He has been very supportive and has given me the opportunity to pursue the research of my interest.

I would like to thank Dr. Stephen Yurkovich for giving me an opportunity to get test data from his Energy Storage Systems Lab. I would also like to thank all my colleagues in the lab who have always helped me.

I would like to thank Dr. Nicholas Gans and Dr. Babak Fahimi for serving on my examination committee.

My deepest gratitude goes to my parents for their constant support and encouragement.

April 2018

RC CIRCUIT MODEL-BASED ANOMALY DETECTION FOR LI-ION BATTERIES

Tunga R, M SEE
The University of Texas at Dallas, 2018

Supervising Professor: Dr. Justin Ruths, Chair

With the increased use of Lithium ion batteries in a variety of applications, the presence of an anomaly proves to be a major concern as it not only affects the battery, but also affects the battery operated system. Battery Management System (BMS) can be equipped with various anomaly detection procedures to detect failures and attacks and hence prevent improper functioning and catastrophic events caused by such anomalies. In this research, the Lithium ion battery is modeled into a first order RC equivalent circuit to understand its behavior. Kalman filter is used to estimate the states and an adaptive estimation algorithm is used to estimate the model parameters. Residual based detection mechanism is employed for anomaly detection. By understanding the performance of the detectors and comparing them with each other, they are tuned to detect the zero-alarm attacks which equip them for worst-case attack detection.

TABLE OF CONTENTS

LIST OF FIGURES

LIST OF TABLES

CHAPTER 1

INTRODUCTION

1.1 Introduction

Increasing energy demands has given rise to the increase in alternatives for fossil fuels. As the combustion of fossil fuels leads to the emission of green house gases which causes global warming, efficient and renewable energy sources are required to satisfy the demand as well as protect the environment. Along with renewable energy sources, energy storage solutions like batteries are the most promising options specially for the on-going huge demand for electric vehicles. They also have applications in portable electronics such as mobile phones and laptops. Li-ion batteries are extensively used among other types of batteries for various applications because of it's advantages.

To maintain the performance of the battery and the battery operated systems, they must be protected from situations that could lead to hazardous effects. Real-time detection of failures and attacks is an important element of maintaining the safety of the battery. Although there has been work in this area, there is much room for improvement. This research work explains the importance of detection of anomalies in batteries and proposes a detection strategy. It focuses on the estimation of the state and model parameters using Kalman filter and an adaptive estimation algorithm. It also explains a variety of detectors, and their tuning procedures for worst case attack detection.

1.2 Thesis outline

In this thesis we implement an anomaly detection mechanism to detect battery failure or sensor attacks and tune the detectors for worst-case attack detection. In the next Chapter, we will talk about batteries and Battery Management Systems. In Chapter 3, we will explain

the modeling of the battery into a first order RC equivalent circuit. In Chapter 4, we will explain the hardware of the battery testing equipment and data generation. In Chapter 5, we use Kalman filter and an adaptive estimation algorithm for state and parameter estimation. In Chapter 6, we will explain the anomaly detection strategy, understand various detectors, compare them with each other and tune them for worst-case attack detection. This Chapter is based on our previous work on Tuning of Windowed Chi-Squared Detectors for Sensor Attacks (Tunga and Justin, 2018). In Chapter 7 we will discuss the distance measure plots for the implementation of the detection mechanism on a Li-ion battery model.

CHAPTER 2

BATTERIES AND BATTERY MANAGEMENT SYSTEM

Lithium is the lightest metal, it has the highest electrochemical potential, and provides the largest specific energy (capacity) per unit weight. It also provides high energy density. But, it also has a few drawbacks. An electrical short can be caused when the dendrites produced on the anode penetrate the separator and overheating is caused when the cell temperature rises and approaches the melting point. These drawbacks along with instability of lithium metal led to a non-metallic, rechargeable solution using Lithium ions. Although the specific energy for lithium-ion is lower than the lithium metal, Li-ion is safe when voltage and current levels are maintained within the safety limits. Extensive research in the cell chemistry has resulted in the reduction of cost, increase in specific energy, low maintenance, and low self-discharge. Hence the Li-ion batteries have been universally acceptable for portable applications and are most widely used among other batteries for electric vehicles.

2.1 Lithium-ion Cell Construction and Operation

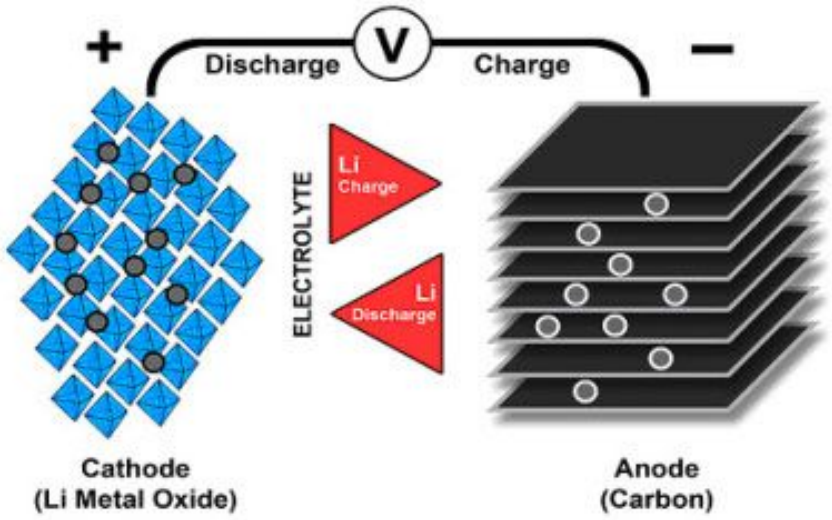

Figure 2.1. Li-ion cell construction (Battery University, 2016)

Figure 2.1 demonstrates the construction of a Li-ion battery. It possesses an anode (negative electrode which is usually made of porous carbon), a cathode (positive electrode) and electrolyte (conductor). During discharge, ions flow from the anode to the cathode through the electrolyte and separator. The direction of the flow of ions is reversed during charge. During discharge, the anode undergoes oxidation and loses electrons which are gained by the cathode. The anode materials offer higher Li-ion storage capacity. This makes the cathode material the limiting factor in the performance of the Li-ion batteries (Liu et al., 2016). Hence the charge capacity and power delivery of the battery is dependent on the cathode material.

2.2 Types of Li-ion cells

A number of varieties of Li-ion batteries exist. For example:

- Lithium Cobalt Oxide (or Lithium Cobaltate)
- Lithium Manganese Oxide (a.k.a Lithium Manganate)
- Lithium Nickel Manganese Cobalt
- Lithium Iron Phosphate
- Lithium Nickel Cobalt Aluminum Oxide
- Lithium Nickel Oxide
- Lithium Titanate

The selection of materials of the positive and negative electrode and the composition of the electrolyte is called battery chemistry. The battery chemistry will have a significant effect on the systems which monitor the battery. The combinations of the cathode and anode materials causes trade-offs between the qualities of the battery. In addition, the performance of

the batteries can be maximized by operating the batteries using an efficient Battery Management System.

Battery Management System (BMS) is an embedded system with electronics and processing designed for a specific application. This may include any of the following functions:

- Monitoring the batteries
- Estimating the internal dynamics of the battery
- Maximizing the performance of the battery
- Reporting and protecting the safety of battery
- Maintaining the battery in a state which can fulfill its functional design requirements

2.3 Applications of BMS

BMS is mostly applied to electric vehicles involving battery packs. However, it also finds its applications in electronic devices. In electric vehicles where battery is the only power source, the BMS should include battery monitoring and protection systems to keep the battery ready to deliver necessary power. Along with thermal management, it should also include systems that control charging (Hu, 2011). Some of the application of BMS include:

- **Battery Electric Vehicle (BEV)**

  BEV uses the chemical energy stored in the battery. For propulsion, it uses electric motors and motor controllers instead of internal combustion engine. As it derives the required power from the battery pack, it does not have an internal combustion engine and fuel tank.

- **Hybrid Electric Vehicle (HEV)**

  HEV combines the internal combustion with an electric propulsion system. This achieves better fuel economy (without compromising its performance) than a conventional vehicle that uses only IC engine. It cannot be plugged-in to charge the battery. Instead it uses regenerative breaking and the internal combustion engine to charge the battery.

- **Plug-in Hybrid Electric Vehicle (PHEV)**

  PHEV is a HEV that can be charged by either plugging into an external power source or by the engine and generator. When the battery is emptied, the conventional engine turns on and the vehicle operates just as a conventional vehicles.

- **Extended Range Electric Vehicle (E-REV)**

  E-REV consists of a plug-in battery, electric motor, and internal combustion engine. The electric motor is responsible for driving the wheels, while the internal combustion engine acts as generator to recharge the battery.

2.4 Fundamental parameters of BMS

- **SOC**: State of Charge (SOC) is the equivalent of fuel gauge for the battery pack used by the load device to determine the available run time. It is also linked to other characteristics such as impedance and power capability.

- **SOH**: State of Health (SOH) indicates the condition of the battery compared to its ideal conditions. It determines the remaining useful life of the battery as it ages.

- **OCV**: Open circuit voltage (OCV) is the potential difference between the electrodes of the battery at steady state i.e. when no current is flowing through the battery.

- **SOC-OCV curve**: The SOC-OCV curve is a one-to-one mapping of SOC and OCV values which can be used to reflect OCV at a given SOC and vice-versa.

- **Power limits**: It indicates the battery's real-time charge and discharge capabilities.

2.5 Factors included in Batteries

1. **Voltage measurement range**:

   As the specific safe working range is different for different chemistries, the voltage measurement range of the battery is optimized to have more precision on the safe working range. The battery management system is modified if the maximum possible measurement does not cover the full range for most of the cell types with appropriate accuracy.

2. **Voltage to SOC relationship**:

   Several factors depend on the shape of the SOC-OCV curve. For example, a flat voltage profile during discharge indicates the requirement of accurate measurement circuit and battery mode for accurate SOC calculation.

3. **Cell internal dynamics**:

   Internal cell dynamics including polarization and hysteresis are affected by the cell design and cell chemistry. For accurate state estimation in cells with long lasting internal polarization, special hardware which is capable of making measurements during long periods of inactivity is required.

4. **Recommended temperature ranges**:

   Temperature accuracy varies over the entire operating range of the cell, but it is important to make accurate measurements around critical transition points.

5. **Self-discharge rate**:

   As the size of the cell balancing systems is related to the self-discharge rate, cell with more variation in self-discharge require more balancing capability.

6. **Cell degradation characteristics**:

   Cell degradation characteristics such as increased cell impedance, increased self-discharge, decreased capacity are caused due to cell aging. A BMS is required to maintain the fundamental performance of the cell.

7. **Safety**:

   Care must be taken to prevent catastrophic conditions caused by reactive cell chemistries. Hence, the cell chemistry, size and other design factors are assessed to avoid the risk of a potential battery management failure.

   Conditions which can lead to an unsafe failure mode of a battery are as follows:

   - **Overcharge**:

     It occurs when a cell is charged to a state of charge (SOC) greater than 100%, which can lead to thermal runaway.

   - **Over-discharge**:

     It occurs when a cell is discharged beyond 0% SOC or 100% depth of discharge (DOD).

   - **High temperature**:

     It can be due to the exposure to high ambient temperatures and abnormal sources of heat, battery overload (overcharge or over-discharge), which leads to internal heating.

   - **Low temperature**:

     Charging at low temperature can lead to an internal short circuit and discharging at low temperature is limited due to increased cell impedance.

- **Overcurrent**:

  Large currents cause internal heating and result in high temperature conditions.

- **Internal cell defects**:

  Internal faults, defects in the cell separator, presence of foreign matter can lead to several undesirable conditions.

- **Mechanical shock, crush, penetration**:

  Mechanical damage to the cells can lead to internal or external short circuit which can result in electrolyte leakage, thermal runaway and shock hazards.

- **Age**:

  One of the conditions causing failure of the batteries with time is age. The probability of failure associated with other conditions increases with age.

2.6 Longevity

The performance of the battery can be reduced due to two main factors:

- **Cycle life**:

  It is the degradation of the battery with each charge/discharge cycle performed.

- **Calendar life**: It is the degradation of the battery strictly as a function of time since manufacturing.

The principle modes of degradation for Li-ion battery cells are:

- **Capacity fade**: It is the decrease in the usable capacity of the battery in-turn reducing the amount of energy the battery can store.

- **Power fade/Impedance growth**: It is the increase in the internal impedance with aging, leading to reduction in the power delivered from the cell.

2.6.1 Factors affecting the longevity of batteries

- **Temperature**: Capacity and power fade can be accelerated by temperature.

- **Operating window**: Operating the battery at intermediate SOC is ideal, because batteries subjected to overcharge and under-charge degrade faster.

BMS is required to control these factors and maintain the performance of the battery by providing accurate and dynamic feedback about the capability of the battery.

2.7 Charge Balancing

Charge balancing, used to account for the differences in cell performance modifies the level of charge in the cells. There are two types of balancing techniques (G.L.Plett, 2015b):

- Active balancing: Moves the charges from cells with high potential to cells with lower potential and conserves the energy in the battery pack.

- Passive balancing: Drains the charges from cells with higher potential and dissipates as heat.

Li-ion batteries are not capable of self-balancing and requires a BMS for proper maintenance of the system. It is also required to balance the cell capacity. For example, without balancing, the effective capacity of the cells in series is limited to the lowest capacity in the series connection of the cells. With charge-transfer balancing, it is possible to transfer charges from high capacity cells to the low capacity cells and increase the effective capacity of the battery. As the cell impedance is dependent on SOC, the cells with different SOC have different power densities. Extreme values of SOC limit the battery power capabilities.

2.8 Battery State Estimation

A Battery Management System (BMS) is required to estimate values that describe the operating conditions of the battery. These include battery state of charge (SOC), power fade and capacity fade (which help in determining the state of health of the battery) and instantaneous available power. It is important for the estimation mechanism to adapt to the changing characteristics and provide accurate estimates of the battery states and parameters. Kalman filter and extended Kalman filter for linear and non-linear systems respectively can be used to estimate the dynamic states of a system.

2.8.1 State of Charge Estimation

The SOC of the cell is the ratio of the remaining capacity to the nominal capacity of the cell, where the remaining capacity is the number of ampere-hours that can be drawn from the cell at room temperature at the C-rate before it is fully discharged and the nominal capacity C_n of the cell is the number of ampere-hours that can be drawn from the cell at room temperature at the C-rate, starting with the cell fully charged. C-rate is the rate at which battery is discharged or charged relative to its nominal capacity (MIT, 2008). SOC is equivalent to providing a fuel gauge to the load device which indicates the estimated remaining run time for an electric vehicle system. However, it does not indicate the fraction of available energy in the battery. The remaining energy in the battery is indicted by the state of energy (SOE). SOE depends directly on the discharge rate which is affected by the internal resistance of the battery. While the state of charge represents the residual charge of the battery, the state-of-energy is integral result of battery power, which is the product of current and terminal voltage (Dong et al., 2015).

The estimation methods for battery packs consider that every single battery cell is uniform in the battery pack (Xiong et al., 2017). But, nonlinear relationships between SOC and

OCV, high coulombic efficiencies and lack of self-balancing leads to divergence in individual cells over the life of a battery system. Hence it is important to have high accuracy in the estimation of SOC for applications involving high energy and high power Li-ion batteries.

Characteristics of the Battery required for SOC estimation

- The capacity of a cell C is the maximum number of ampere-hours that can be drawn from the cell before it is fully discharged, at room temperature, starting with the cell fully charged. Capacity reduces non-linearly with changes in temperature (G.L.Plett, 2015a).

- Coulombic efficiency of a Li-ion battery describes the charge efficiency by which the electrons are transferred. Mathematically, it is the ratio of the total charge extracted from the battery to the total charge put into the battery over one full cycle. It can be modeled by using a factor η, as follows:

$$\begin{cases} \text{During charge :} & \dfrac{dSOC}{dt} = \eta \dfrac{1}{C} I \quad (0 < \eta < 1) \\ \text{During discharge :} & \dfrac{dSOC}{dt} = \dfrac{1}{C} I \end{cases} \tag{2.1}$$

- The terminal voltage includes the effect of hysteresis and polarization.

Coulomb Counting method

The coulomb counting method is also known as ampere hour counting or current integration method. It uses battery current readings to integrate over time to calculate SOC values. It is given by:

$$SOC(t) = SOC(t_0) + \frac{1}{C} \int_{t_0}^{t_0+\tau} (I - I_{loss}) dt \tag{2.2}$$

where, $SOC(t_0)$ is the initial SOC, C is the nominal capacity of the battery, I is the battery current and I_{loss} is the current consumed due to certain loss reactions.

This method calculates the remaining capacity in the battery by accumulating the charge transferred in or out of the battery (Murnane and Ghazel, 2017). It is important to have an accurate estimate of the initial SOC value for the coulomb counting method to be accurate. Inaccurate initial SOC measurements, self-discharge, and the losses during charging and discharging will lead to large errors.

Voltage/ OCV Method

The OCV method converts a terminal voltage reading of the battery to its equivalent SOC value using the SOC-OCV curve obtained by charge and discharge cycles of the battery. The inaccuracy in this method is because of the effect the cell materials and temperature can have on the voltage. Error occurs when the battery is disturbed by charging or discharging during the estimation. Hence, to obtain accurate readings it is necessary to rest the battery for a long duration. This makes the OCV method not applicable for an active battery.

Kalman filter method

The Kalman filter can be used to estimate the SOC of a battery. It is an optimal method for SOC estimation because, it not only estimates the internal states, but also provides the dynamic error bounds on its state estimates. It is a model based estimation technique where the Li-ion cell is modeled as a state-space system. It employs an error correction mechanism to provide real-time predictions of the SOC. (Murnane and Ghazel, 2017) For accurate estimation of the states, it requires an accurate model and accurate initialization. To account for the non-linear behavior of the SOC with the battery output voltage, the extended Kalman filter is used with a linearization procedure.

2.8.2 State of Health estimation

Battery state of health (SOH) is the condition of the battery from the beginning of life to its end of life. Capacity fade, power fade or impedance growth, increased self-discharge are the

main factors indicating the reduction in the health of the battery. Battery capability fade is a function of the charge and discharge cycles (cycle life) and time (calendar life). The decrease in the capacity of the battery as it ages is termed as capacity fade. Inability of the Li-ions or the electrons to reach the active metal site causes capacity fade. This can be due to the damage of the electrode structure. The capacity fade also affects the SOC-OCV relationship.

The equivalent series resistance of the battery increases with the age of the battery which can be due to structural deterioration. This increase in resistance in the cell can be referred to as the power fade. Soild-electrolyte interphase (SEI) growth which occurs in batteries using a carbon anode, causes the loss of active material and reduction in surface area which results in increase of the impedance or resistance during aging.

Aging also increases the self-discharge rate which reduces the life of the battery.
The overall state of health of the battery can be computed using these three factors:
SOH = SOH(capacity fade, power fade, self-discharge) (Weicker, 2014)

At the beginning of life of the battery the SOH is considered as 100%. SOH of the battery reduces linearly when the charge/ discharge profile is identical under identical environment conditions. But under extreme operations, the decrease in SOH is not linear. The battery management system (BMS) is responsible for the dynamic estimation of the factors affecting the battery SOH. Given the nonlinear (relationship between SOC and OCV), non-exact (battery model does completely model the performance of the cell) and non-stationary (mode parameters continuously change with SOC) behavior of the battery, it is challenging to estimate the battery SOH.

2.9 Anomaly Detection

One of the functions of BMS is to ensure the safety of a battery. Hence, the battery management system is required to detect anomalies in the battery cells. It is important for these anomaly detection mechanisms to be accurate and robust for the BMS to be reliable. Anomalies can be attributed to failures in the battery cells or to attacks on the sensors. For example, a current sensor fault can lead to error in the SOC estimation which can lead to the improper functioning of the BMS and fault in the temperature sensor might lead to improper thermal management. Some of reasons for battery failure include:

- **Overcharge/ Over-voltage**

  Overcharge can lead to catastrophic effects on the battery operated system. When overcharge occurs, the BMS should respond immediately and disconnect the battery from the system. During overcharge there is a significant difference in the battery voltage in comparison to it's voltage under normal operation. Setting a threshold on the maximum expected voltage with respect to current helps in determining fault or failure.

- **Over-discharge**

  Over-discharge can reduce the cell voltage to nearly zero or very low values which can be below the minimum voltage limit. The BMS should allow the measurement for a high-voltage stack at different levels of granularity to determine if the voltage reading is due to a broken connection. Because the broken wire case is less severe than a short-circuited or fully discharged cell and detection of this type of failure can prevent a battery shutdown and loss of functionality.

- **Over-temperature**

  Thermal management is necessary to maintain the temperature of the battery within the safety limits. Over-temperature conditions leads to the shut-down of the system.

- **Over-current**

  Oversizing the fuse in order to allow higher current and more energy before blowing the fuse is a possible reason for the battery components to be exposed to over-currents. In such cases, the BMS should manage the trade-off and allow high current for sufficient duration without overcharging the battery. It is necessary to have an ideal measurement range for the current sensor to make accurate and precise current measurements.

- **Battery Imbalance/ Excessive Self-discharge**

  Battery imbalance occurs when the cell balancing system cannot compensate for the excessive self-discharge in the cells. The maximum expected voltage difference between the cells can be determined using the slope of the SOC-OCV relationship and the imbalance in the cells should not exceed the limit. The imbalance and self-discharge can be easily determined if the SOC and capacity of individual cells is known.

- **Internal Short-circuit**

  Detection of internal short-circuit is important to prevent thermal runaway and abnormal depletion of SOC in batteries.

- **Excessive Capacity Loss**

  While capacity fade is typically due to the aging, capacity loss can be due to a fault or failure. It is important to know the distinction between capacity fade and abnormal capacity loss. Capacity loss is most often attributed to the excessive and uncontrolled self-discharge in the cells. Significant and unexpected capacity loss may indicate a serious internal defect due to internal shorts, cell damage, or lithium plating.

The content from this chapter is mostly based on the book (Weicker, 2014).

2.10 Sensor Attacks on Lithium-ion Batteries or Battery Packs

Battery Management Systems (BMS) plays an important role in the maintaining the performance of the battery. In addition to this, the security of the battery systems is necessary for the proper functioning of the battery and prevent the battery from failure, thermal runaway, explosion, and other battery threats. Detection procedures must be incorporated into the system to ensure its efficiency. Battery security is an important aspect of Battery Controls and BMS. In the case of a battery operated system, the attacks initiated from one layer affect the other layers and this is called "cross-layer attacks". Batteries can also be a part of a Cyber-Physical System (CPS).

In a battery system, the sensors connected to the battery cells are responsible for collecting the values of current, voltage, and temperature. These values along with the battery parameters are used by the BMS to monitor and protect the battery from thermal runaway, over-charging, under-charging etc. When these parameters exceed the safety limits, unsafe or catastrophic operations take place. This can be caused by a fault in the battery or even by an external attack.

The sensor attacks include modifying the sensor measured data, overcharging, undercharging, draining, information leakage etc. Attacks can be on the availability, integrity and confidentiality of data. Through some unique application layer features, indirect attacks on the battery system can be implemented. For example, the regenerative braking system can be disabled or heating-ventilation-air-conditioning (HVAC) can be altered without the notice of the passenger. These attacks drain the battery and therefore affect their availability.
Another type of attack is spoof the sensor information which is sent to the control unit via the intra-network which leads to draining of the battery. Apart from spoofing the critical

resources, an attacker can also spoof the critical information which can cause the battery operated system to drain out more power from the battery, which can lead to deep discharge. The Electric Vehicles (EV) are prone to such vulnerabilities because of the high levels of autonomous processing and interconnectivity in them. The attackers are also capable of stealthily forge the data of the battery or display incorrect information about the battery state (SOC and SOH) which can lead to damage of the battery and electric vehicle.

CHAPTER 3

BATTERY MODEL IMPLEMENTATION

3.1 Battery Models

Battery models are required to be accurate to capture the dynamics of the battery and predict its performance. Types of battery models include:

1. **Electrochemical models**:

   Electrochemical model deals with the physical design of the battery and the electrochemical reactions in the electrodes and electrolyte.

2. **Mathematical models**: Mathematical models do not provide the voltage-current relationship of a battery. They are generally used to predict the run-time characteristics of a battery. Mathematical models are relatively easy to compute but are less accurate and are application specific. Some of the mathematical models include:

   - Shepherd model
   - Unnewehr universal model
   - Nernst model

3. **Equivalent circuit models**: Equivalent circuit models use voltage sources, resistors and capacitors to measure battery performance. They have higher accuracy compared to mathematical models and requires lower computational effort compared to electrochemical models. They can be easily implemented in BMS to dynamically predict the battery voltage. Some of the equivalent circuit models include:

   - Thevenin Model
   - PNGV Model

- DP Model
- RC model

3.2 State Space Model for First Order RC Equivalent Circuit

In this research, we consider an **RC model** of the Li-ion battery. This model consists of an RC network in series with the internal resistance. The voltage source represents the open circuit voltage, the parallel RC networks represent the delay in voltage response. In this thesis we are considering a Randles circuit which is a first order RC equivalent circuit. However, increasing the number of RC branches beyond two does not provide significant improvement in accuracy. The model parameters are as follows:

- **Internal resistance** (R_s): It is dependent on SOC, temperature and discharge current. This internal resistance is the cause for the voltage drop at the beginning of a discharge process.

- **Open circuit voltage** (OCV): It is the voltage across the electrodes of a battery in the absence of either charge or discharge current. It varies non-linearly with SOC.

- **RC branch** (R_t, C_t): It is the parallel resistor-capacitor network. This network is the cause for the slow recovery of the battery voltage to its open circuit voltage

- **Battery terminal voltage** (v_{cell}): It is the measured output voltage at the load. It is obtained by subtracting the voltage drop across the RC network and internal resistance from the open circuit voltage.

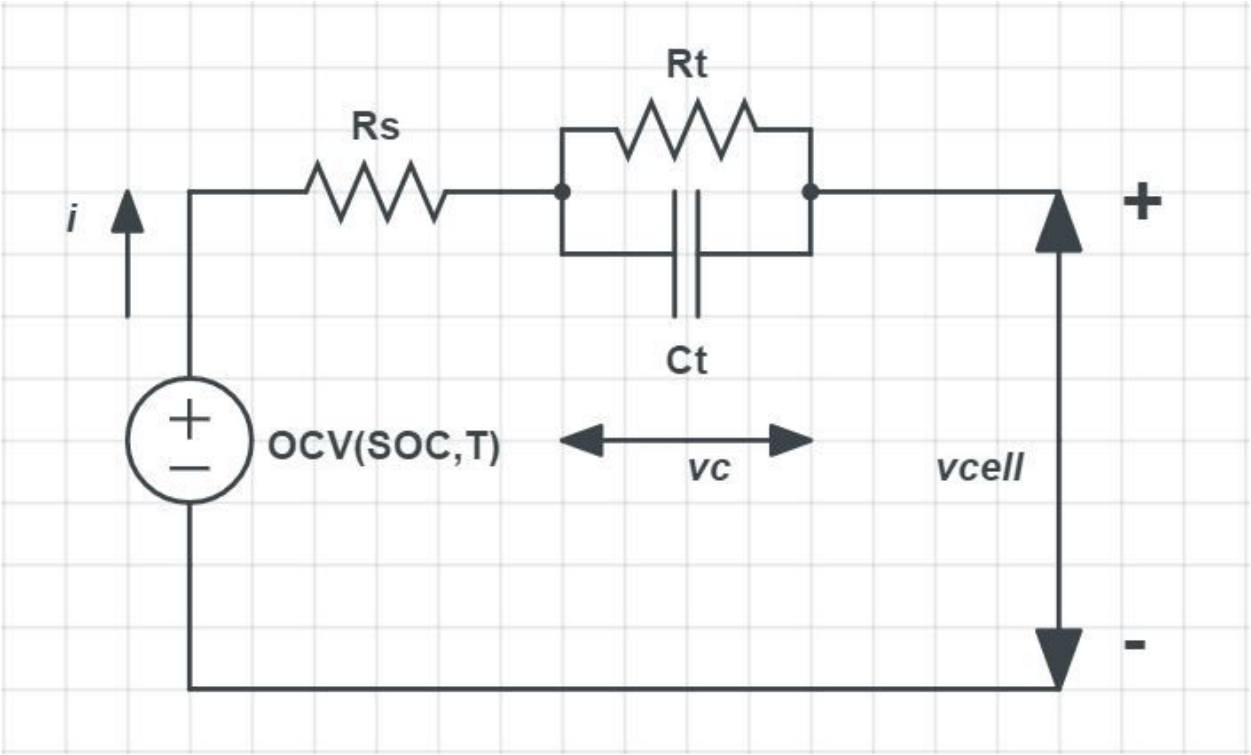

Figure 3.1. Randles circuit

The Li-ion battery cell can be modeled into an equivalent circuit (as shown in Figure 3.1) to understand the behavior and response of the cell to various conditions. The simplest possible model of an ideal battery is an ideal voltage source, but this model is inadequate. To improve the model it is necessary to include a dependence on the charge status of the cell (i.e. SOC) (G.L.Plett, 2015b). The voltage of the cell drops under the influence of load, i.e., the cell's terminal voltage reduces from the open circuit voltage (OCV) due to the flow of current in the circuit and this phenomenon is termed as polarization. This can be modeled in part as a resistance in series with the ideal voltage source.

$$v_{cell} = OCV(SOC) - iR_s \tag{3.1}$$

This models an instantaneous response to change in input current. When the cell is allowed to rest, the voltage does not immediately return to OCV. This slowly changing voltage is

referred to as diffusion voltage. This can be approximated by using one or more parallel RC network in series with the resistance R_s. Then the cell voltage is modeled as:

$$v_{cell} = OCV(SOC) - iR_s - v_c \tag{3.2}$$

where $v_c(t)$ is the voltage across the RC network. Thus, this forms the output equation of the system. The differential voltage across the RC network which forms the state equation is given as follows:

$$\dot{v_c} = \frac{-1}{R_t C_t} v_c + \frac{1}{C_t} i \tag{3.3}$$

Thus the continuous-time state space representation of the Li-ion battery is given as follows:

$$\begin{cases} \dot{v_c} = \dfrac{-1}{R_t C_t} v_c + \dfrac{1}{C_t} i \\ v_{cell} = OCV(SOC) - iR_s - v_c \end{cases} \tag{3.4}$$

The following section explains the conversion of this continuous-time system to a discrete-time system. The current through the capacitor C_t in the RC network can be expressed as:

$$i_c(t) = C_t \dot{v_c}(t) \tag{3.5}$$

The current flowing through the circuit is expressed as:

$$i_{cell}(t) = i_c(t) + i_{R_s}(t) \tag{3.6}$$

Since $v_c(t) = R_t i_{R_t}(t)$, the current equation can be written as:

$$\begin{cases} i_{cell}(t) = i_{R_t}(t) + R_t C_t \dfrac{di_{R_t}}{dt} \\ \dfrac{di_{R_t}}{dt} = -\dfrac{1}{R_t C_t} i_{R_t}(t) + \dfrac{1}{R_t C_t} i_{cell}(t). \end{cases} \tag{3.7}$$

These continuous-time ordinary differential equations are converted into discrete-time ordinary difference equations. Generically, it can be derived as follows: The solution to an ordinary differential equation can be given as:

$$\begin{cases} \dot{x}(t) = ax(t) + bu(t) \\ \dot{x}(t) - ax(t) = bu(t) \\ e^{-at}[\dot{x}(t) - ax(t)] = \dfrac{d}{dt}[e^{-at}\dot{x}(t)] \\ \dfrac{d}{dt}[e^{-at}\dot{x}(t)] = e^{-at}bu(t). \end{cases} \tag{3.8}$$

Let $x[t]$ at discrete time be defined as $x[k] := x[k\Delta t]$ Then:

$$\begin{cases} x[k+1] = & x((k+1)\Delta t) \\ x[k+1] = & e^{a(k+1)\Delta t}x(0) + \displaystyle\int_0^{k+1} e^{a((k+1)\Delta t - \tau)} \quad bu(\tau) \quad d\tau \\ x[k+1] = & e^{a(k+1)\Delta t}x(0) + \displaystyle\int_0^{k} e^{a((k+1)\Delta t - \tau)} \quad bu(\tau) \quad d\tau + \int_{k\Delta t}^{(k+1)\Delta} e^{a((k+1)\Delta t - \tau)} \quad bu(\tau) \quad d\tau \\ x[k+1] = & e^{a\Delta t}e^{a(k)\Delta t}x(0) + \displaystyle\int_0^{k} e^{a((k+1)\Delta t - \tau)} \quad bu(\tau) \quad d\tau + \int_{k\Delta t}^{(k+1)\Delta} e^{a((k+1)\Delta t - \tau)} \quad bu(\tau) \quad d\tau \\ x[k+1] = & e^{a\Delta t}x(k\Delta t) + \displaystyle\int_{k\Delta t}^{(k+1)\Delta} e^{a((k+1)\Delta t - \tau)} \quad bu(\tau) \quad d\tau \\ x[k+1] = & e^{a\Delta t}x[k] + \displaystyle\int_{k\Delta t}^{(k+1)\Delta} e^{a((k+1)\Delta t - \tau)} \quad bu(\tau) \quad d\tau \end{cases} \tag{3.9}$$

Assuming $u(\tau)$ is a constant from $k\Delta t$ to $(k+1)\Delta t$ and equal to $u(k\Delta t)$

$$\begin{cases} x[k+1] = & e^{a\Delta t}x[k] + e^{a(k+1)\Delta t}\left(\displaystyle\int_{k\Delta t}^{(k+1)\Delta} e^{a\tau}\right) \quad bu(k) \\ x[k+1] = & e^{a\Delta t}x[k] + \dfrac{1}{a}e^{a(k+1)\Delta t}\left(e^{-ak\tau t} - e^{a(k+1)\Delta t}\right) \quad bu(k) \\ x[k+1] = & e^{a\Delta t}x[k] + \dfrac{1}{a}\left(e^{a(k+1)\Delta t} - 1\right) \quad bu(k) \end{cases} \tag{3.10}$$

Applying this result to the ODE describing the RC circuit:

$$a = -\frac{1}{R_t C_t}, \quad b = \frac{1}{R_t C_t}, \quad x[k] = i_{R_t}[k] \quad u[k] = i[k] \tag{3.11}$$

Substituting these values into the generic result, we get:

$$i_{R_t}[k+1] = exp\left(\frac{-\Delta t}{R_t C_t}\right) i_{R_t}[k] + \left(1 - exp\left(\frac{-\Delta t}{R_t C_t}\right)\right) i[k] \tag{3.12}$$

Since $v_c(t) = R_t i_{R_t}(t)$, 3.12 can be written as:

$$v_c[k+1] = exp\left(\frac{-\Delta t}{R_t C_t}\right) v_c[k] + R_t\left(1 - exp\left(\frac{-\Delta t}{R_t C_t}\right)\right) i[k] \tag{3.13}$$

Hence, the discrete-time state space representation of the Li-ion battery is given by:

$$\begin{cases} v_c[k+1] = exp\left(\frac{-\Delta t}{R_t C_t}\right) v_c[k] + R_t\left(1 - exp\left(\frac{-\Delta t}{R_t C_t}\right)\right) i[k] \\ \quad v_{cell}[k] = OCV(SOC[k]) - i[k]R_s - v_c[k] \end{cases} \tag{3.14}$$

CHAPTER 4

BATTERY TESTING

Sufficient data is required for the estimation of states and parameters of the model. Various tests are run on the battery to obtain the testing data for this research. These tests provide a voltage profile for the input current profile.

To perform the tests and generate the testing data, a battery pack manufactured by Turnigy has been used. To minimize resistance and sustain high current loads, Turnigy batteries are equipped with heavy duty discharge leads. Each pack is equipped with gold plated connectors and JST-XH style balance connectors. All Turnigy Li-polymer batteries packs are assembled using IR matched cells.
The specifications of the battery are as follows (Turnigy, 2018):

- Minimum Capacity: 2200mAh
- Configuration: 3S1P / 11.1v / 3Cell
- Constant Discharge: 25C
- Peak Discharge (10sec): 35C
- Pack Weight: 188g
- Pack Size: 105 x 33 x 24mm
- Charge Plug: JST-XH
- Discharge plug: XT60

The rated capacity of the battery is 2.2Ah. However, the initial capacity of the battery was 1.9537Ah and after ten cycles of mRPT tests (at 25 degree centigrade) the capacity dropped to 0.5940Ah.

4.1 Test Equipment

To obtain the test data, the battery tests were run on an equipment called the cycling station which is shown in Figure 4.1. It consists of a temperature chamber and associated software tools. The cycling station was assembled by Car Technologies, LLC. It is a company which performs testing and development of vehicle electrification technologies in close collaboration with The Ohio State University Center for Automotive Research (OSU-CAR).

4.1.1 Cycling Station

The cycling station is used to charge and discharge batteries or battery packs for a given current profile subject to a particular type of battery test. The specific control software present in the cycling station performs the task of a battery management system (BMS). It is responsible for maintaining proper operation of the system by keeping the batteries within the safe operating range. This also protects the cycling station from failures leading to catastrophic conditions. For example, high currents involved in charging or discharging can lead to high temperature conditions like over-heating and thermal runaway. Failures in the battery associated to over-charge, over-discharge, high and low temperatures, and internal cell defects can lead to catastrophic conditions. In such cases the software triggers an emergency stop (E-Stop) which shuts down the system and prevents any damage the battery can cause to the cycling station.

Figure 4.1. Cycling station

The hardware of the cycling station mainly consists of the following:

1. **HP Server**

   To run the customized software for controlling the power supply, load and data acquisition device a HP server is used. It is operated on Red Hat Linux system.

2. **TDK Lambda GEN8-400**

   It is the programmable DC power supply which provides high power density. It used for charging the battery cell or battery pack depending on the configuration. Each supply can have a maximum output voltage of 8V at 400A. Its rated power is 3200 watts. In the cycling station, two of these are connected in series to provide a maximum voltage of 16V at 400A.

3. **Kepco EL 3k-25-400DG**

   It is a modular, air-cooled, electronic load used to test DC power sources such as batteries. It is used for discharging the battery. Kepco Model EL 3K-25-400DG Electronic Load allows the device to operate at 25 volts, it is rated at a maximum current capability of 400 amperes and a power rating of 3000 Watts. The suffix D represents a dual model which contains two identical and independent channels in a single chassis (Kepco Inc., 2012).

4. **NI USB-6008**

   NI USB-6008 is a multifunction data acquisition device (DAQ) which is manufactured by National Instruments. The device features a lightweight mechanical enclosure and is bus powered for easy portability. The metal box minimizes the magnetic interference from other devices. Sensors and signals can be easily connected to the USB6008 with screw-terminal connectivity. The included NIDAQmx driver and configuration utility simplify configuration and measurements. The DAQ is used to sample the voltage,

current and temperature. The sampled values are fed back to the server where the cycler software evaluates the data and plots the real time sampling result. This feedback data can also be used to determine the E-Stop conditions and prevent catastrophic conditions (USB-6008, 2018).

5. **Type T Thermocouple**

   Type T Thermocouple is the temperature sensor used in the thermal chamber of the cycling station. It is a very stable thermocouple. It is used to record the thermal behavior of the battery for charge and discharge cycles on the sampled data. It is often used in critical temperature conditions and is mainly used to determine if the temperature exceeds the safe operating range and turns on the E-Stop to terminate the operation.

4.1.2 Thermal Chamber

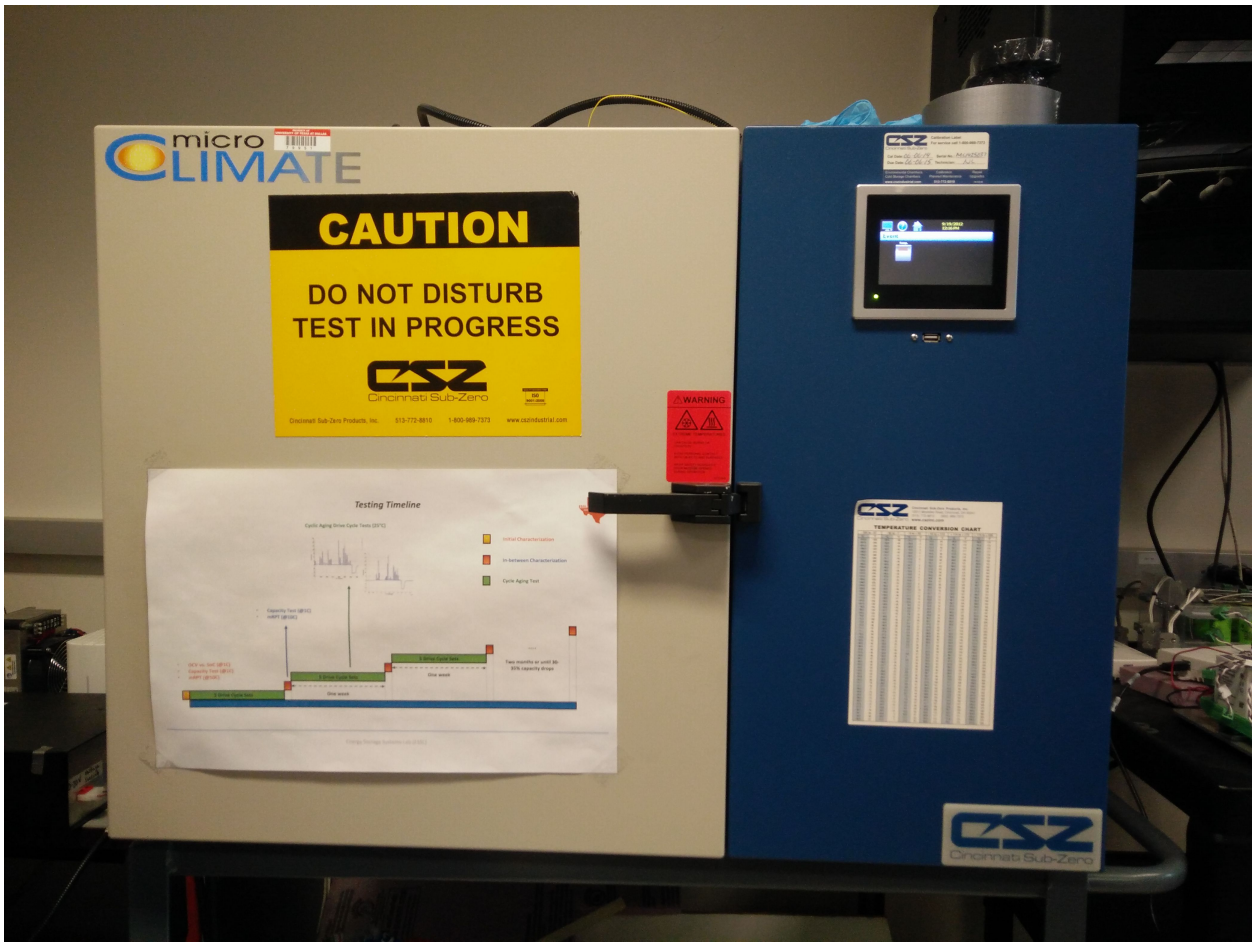

Figure 4.2. Thermal chamber

The tests on the battery are to be carried out at constant temperature. To maintain a constant temperature throughout the test, a thermal chamber is used.

The temperature chamber shown in Figure 4.2 used for testing purposes is the Cincinnati Sub-Zero (CSZ), MicroClimate® Benchtop Test Chamber. The test chamber is capable of simulating a full range of temperature and humidity conditions. Some of the standard features are Solid State Humidity Sensor, RS-232 Computer Interface, Ethernet Control and Monitoring, EZT-430i Touch Screen Controller.

The specifications are as follows:

1. Temperature range:
    - Single Stage: -30°C to +190°C (-22°F to +375°F)
    - Cascade: -70°C to +190°C (-94°F to +375°F)
2. Optimal humidity range: 10% to 95% RH

The lithium ion cell is first fixed into the Peltier junction and then the junction is placed in the temperature chamber. The cables from the cycling station including the power cables for current flow, voltage sensing cables and the thermocouple are inserted into the chamber from the left side of the chamber through a hole and connected to the cell. To eliminate leakage, isolation is achieved using some soft isolation materials like a sponge.

4.2 Battery Data Generation

The battery data generation equipment utilizes a special purpose software and high accuracy instrumentation with a thermal chamber for control of ambient temperatures. Customized profiles run automated charge-discharge cycles on the battery pack. The testing profiles cycle the battery from beginning of life (BOL) to end of life (EOL). Each cycle consists of three test profiles:

1. **Characterization test**:

    Characterization test (Q_i) consists of three parts. The first part is a discharge phase where the battery is discharged at 1C (2.2 A) rate till it reaches the rated minimum voltage. The second part consists of a 30-minute rest phase. The last portion of the test is the charge phase, in which the battery is charged at 1C (-2.2A) rate in CC-CV (constant current constant voltage) mode. Characterization test is used to calculate

the SOC-OCV curve and the capacity of the battery. The below Figure 4.3 illustrates the current and voltage profiles of a characterization test.

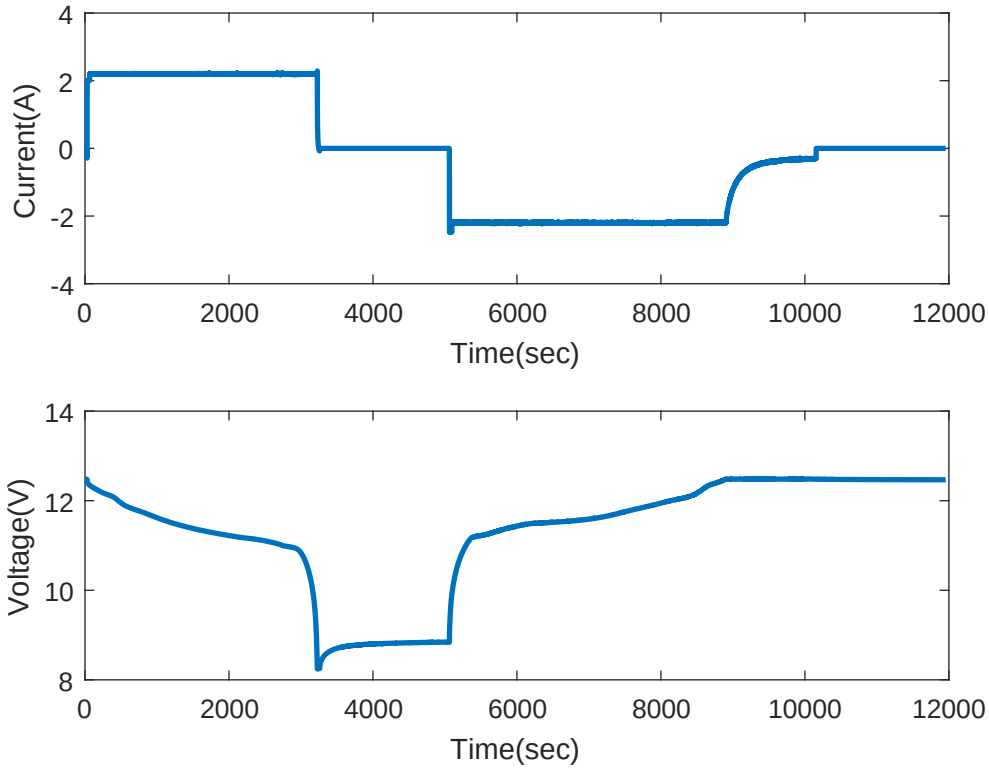

Figure 4.3. Characterization test

2. **Drive cycle test**: The primary purpose of drive cycle test (CC-pulse test) is to age the battery quickly. The pulses try to recreate the effect of an actual drive cycle on a battery in an EV or HEV. There are six pulses in a single set, which is repeated eight times. The first three pulses discharge the battery at 10C, 20C, 10C to 60%, 40% & 20% SOC respectively. The last three pulses charge the battery at 1C, 5C, 1C to 26%, 96% & 100% SOC respectively. There is a three-minute rest period between every discharge and charge pulse set. The below Figure 4.4 illustrates the current and voltage profiles of a drive cycle test.

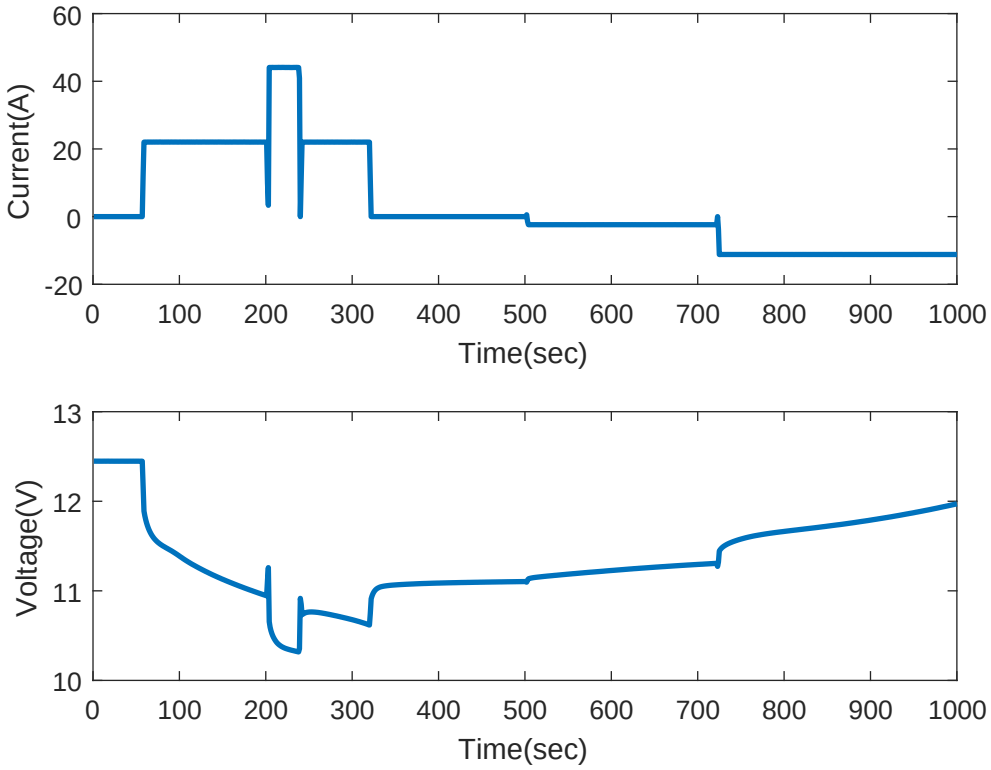

Figure 4.4. Drive cycle test

3. **mini Reference Performance Test (mRPT)**:

   Pulse mini reference point tests or pulse mRPTs consists of five pulses which discharge the battery at 10C (22 A) rate with each pulse responsible for discharging 10% SOC of the battery. There is a 30-minute rest period between every pulse and at the end of fifth pulse the SOC is at 50%. The battery is then charged at a 5C (-11 A) rate in CC-CV mode till the SOC is back up to 100%. The battery response to the pulse is used to calculate the battery parameters. The below Figure 4.5 illustrates the current and voltage profiles of a drive cycle test.

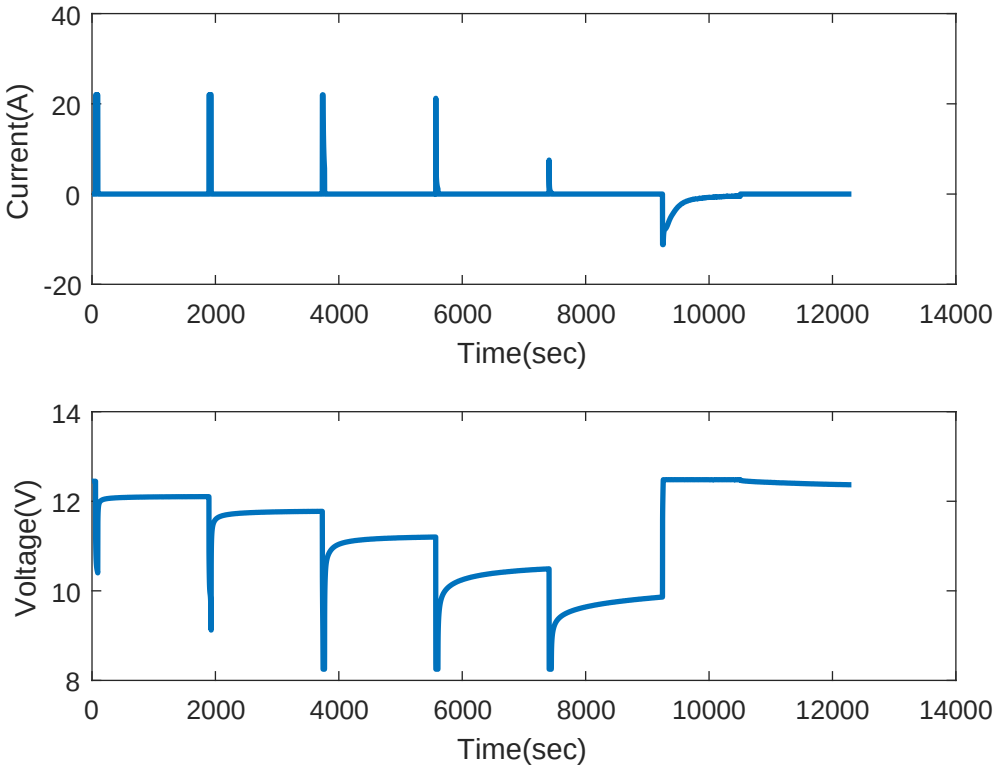

Figure 4.5. mini Reference Performance Test

In particular, for this thesis, test data obtained from the mini Reference Performance Test (mRPT) with five discharge pulses at 10C rate (with 22A of current) (3) has been used.

CHAPTER 5

BATTERY STATE AND PARAMETER ESTIMATION

5.1 Kalman Filter

Kalman filter is a tool used to determine the internal state of a dynamic system. It has been used in many fields including: target tracking, global positioning, dynamic systems control, navigation,and communication. In the battery field it can be used in determining SOC and SOH by using the electrical and thermal conditions of the battery.

The state space representation of a linear dynamic system is given by:

$$\begin{cases} x_{k+1} = Ax_k + Bu_k + w_k, \\ y_k = Cx_k + \eta_k, \end{cases} \tag{5.1}$$

x_k: System state vector at time k

u_k: Known input to the system

w_k: Disturbance or process noise (unknown input that effects the state)

y_k: Measured output

v_k: Measurement noise or sensor noise

A, B, C: Matrices specific to the system that describes its dynamic behavior

In (5.1), the first equation refers to the state or process equation which describes the evolution of states over time and the second equation refers to the output equation which describe the reaction between sates and the measured output.

5.1.1 Working of Kalman Filter

Kalman filter is an estimator used to estimate the state vector x_k using the past measurements y_0, y_1 .... y_k. It basically involves the repetition of two high-level steps: **Prediction** and **Estimation**. Different estimators for the states can be derived depending on the

available measurements. For a linear system, Kalman filter is the optimal minimum-mean-squared-error and maximum-likelihood estimator.

Considering the state space form (5.1), we assume that w_k and η_k are mutually uncorrelated white Gaussian random processes, with zero mean and covariance matrices:

$$E[w_k w_n^T] = \begin{cases} Q_k, & k = n \\ 0, & k \neq n \end{cases} \tag{5.2}$$

$$E[\eta_k \eta_n^T] = \begin{cases} R_k, & k = l \\ 0, & k \neq n \end{cases} \tag{5.3}$$

and $E[w_k \eta_n^T] = 0$ for all values of k.

State estimate time update is given by:

$$\hat{x}_{k+1} = A_k \hat{x}_k + B_k u_k \tag{5.4}$$

The covariance of the estimation error is given by:

$$\begin{cases} \Sigma_{k+1} = E[(x_{k+1} - \hat{x}_{k+1})(x_{k+1} - \hat{x}_{k+1})^T] \\ \Sigma_{k+1} = A_k E[(x_k - \hat{x}_k)(x_k - \hat{x}_k)^T] A_k^T + E[w_k w_k^T] \\ \Sigma_{k+1} = A_k \Sigma_k A_k^T + Q_k \end{cases} \tag{5.5}$$

Hence, Σ_k can be expressed as:

$$\Sigma_k = A_{k-1} \Sigma_{k-1} A_{k-1}^T + Q_k \tag{5.6}$$

We assume that the estimate is the weighted sum of the prediction and the measurement y_k:

$$\hat{x}_{k+1} = K_{k+1}^T \hat{x}_{k+1} + K_{k+1} \hat{y}_{k+1} \tag{5.7}$$

Where K_{k+1}^T and K_{k+1} are the gains. This gain should minimize the conditional mean squared estimation error $e_k = \hat{x}_{k+1} - x_{k+1}$. The Kalman filter gain is given by:

$$K_k = (A_k \Sigma_k C_k^T)(R_k + C_k \Sigma_k C_k^T)^{-}1 \tag{5.8}$$

The unbiased condition is given by:

$$\begin{cases} E[\hat{x}_{k+1}] = E[A_k \hat{x}_k + B u_k] \\ E[\hat{x}_{k+1}] = A_k E[\hat{x}_k] + B u_k \\ E[\hat{x}_{k+1}] = E[x_{k+1}] \end{cases} \tag{5.9}$$

$$\begin{cases} E[\hat{x}_{k+1}] = E[K_{k+1}^T \hat{x}_{k+1} + K_{k+1} C_{k+1} x_{k+1} + K_{k+1} \eta_{k+1}] \\ E[\hat{x}_{k+1}] = K_{k+1}^T E[\hat{x}_{k+1}] + K_{k+1} C_{k+1} E[x_{k+1}] + K_{k+1} E[\eta_{k+1}] \\ E[\hat{x}_{k+1}] = K_{k+1}^T E[\hat{x}_{k+1}] + K_{k+1} C_{k+1} E[x_{k+1}] \end{cases} \tag{5.10}$$

because $E[\eta_{k+1}] = 0$. Using the unbiased condition (5.9) in (5.10), it can be expressed as:

$$\begin{cases} E[\hat{x}_{k+1}] = (K_{k+1}^T + K_{k+1} C_{k+1}) E[x_{k+1}] \\ I = K_{k+1}^T + K_{k+1} C_{k+1} \\ K_{k+1}^T = I - K_{k+1} C_{k+1} \end{cases} \tag{5.11}$$

Substituting (5.11) in (5.7) we obtain:

$$\hat{x}_{k+1} = \begin{cases} (I - K_{k+1} C_{k+1}) \hat{x}_{k+1} + K_{k+1} y_{k+1} \\ \hat{x}_{k+1} + K_{k+1} [y_{k+1} - C_{k+1} \hat{x}_{k+1}] \end{cases} \tag{5.12}$$

Hence, the state estimate equation is:

$$\hat{x}_k = \hat{x}_{k+1} + K_{k+1} [y_{k+1} - C_{k+1} \hat{x}_{k+1}] \tag{5.13}$$

5.2 State estimation using Kalman filter

In this section, a linear Kalman filter is used to estimate the state of the system which is in-turn used to estimate the output voltage. The voltage drop across the RC branch v_c in the battery is considered as the sate x_k, the current i in the battery is the input u_k, and the terminal voltage v_{cell} follows the KVL and forms the output equation. Here we are considering a scalar system. The estimated state v_c is used in the output equation along with the measured voltage v_{cell} and model parameters to estimate the battery output voltage. This estimated output voltage is then compared with the measured terminal voltage. This is further used to determine the residual and distance measure to indicate an anomaly.

5.2.1 State estimation using Kalman filter with fixed model parameters

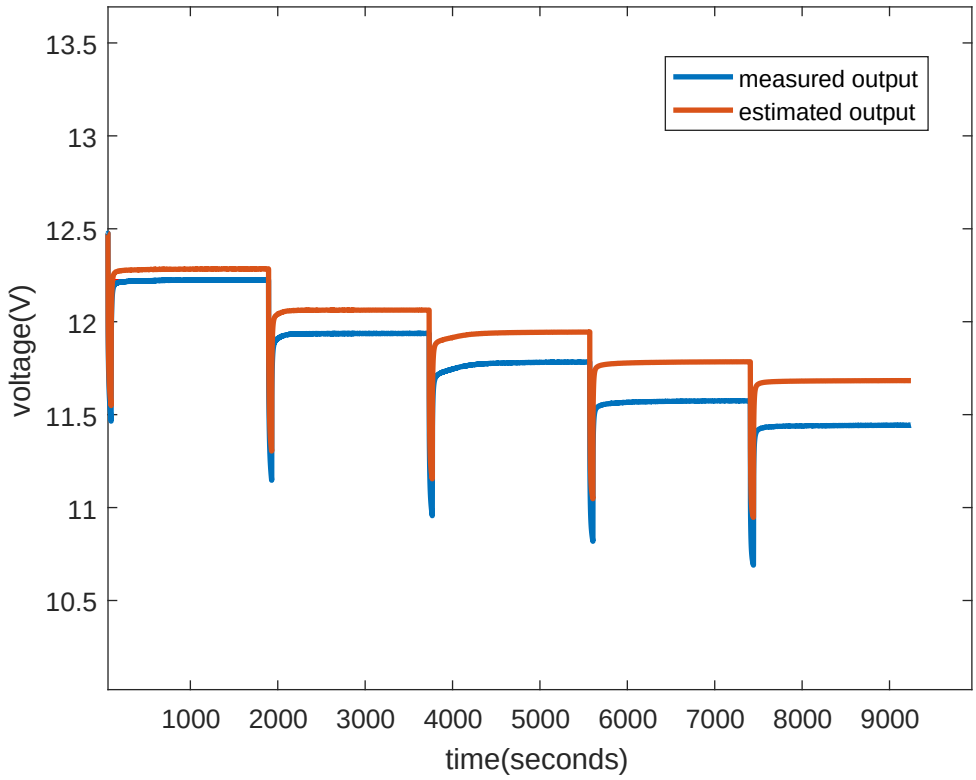

Figure 5.1. Static estimator

Considering the model at 100% SOC, Kalman filter is deployed to estimate the battery terminal voltage. Figure 5.1 illustrates that the estimated voltage does not closely follow the actual measured output. In mRPT tests each pulse reduces the SOC by 10% which also changes the model parameters. This dependence of the model parameters on the changing state of charge is the reason for large estimation error i.e. the difference between the estimated voltage and measured voltage. Updating the model parameters with the changing SOC gives a better performance of the estimator i.e. reduces the estimation error. The model parameters are calculated from the output voltage profile. Figure 5.2 shows the voltage response for a discharge current pulse. This shows the behavior of the battery attributed to resistance, capacitance, and open circuit voltage (OCV) values. In Figure 5.2, the sudden drop of voltage at the start of the discharge current is related to the internal resistance. This series resistance (R_s) is calculated using the change in voltage and the current during discharge. The slow diffusion of voltage before recovery is related to the RC branch. The values of R_t and C_t is calculated using a parameter estimation process. Allowing the battery to rest for long hours and using the change in the steady-state voltage the OCV values can be calculated. This is based on the charge and discharge curve under 1C current condition. Initially, the SOC values are measured using the CC/CV charge and discharge test. The array of data obtained from the discharge curve is flipped to obtain the corresponding data of the charge curve. The OCV values are estimated by calculating the mean difference between the charge and discharge curves. The curve is then normalized to fit the varying SOC. These estimation processes are carried out for the mRPT profile and the corresponding model parameters for the changing values of SOC are obtained which is recored in the table (5.2.1).

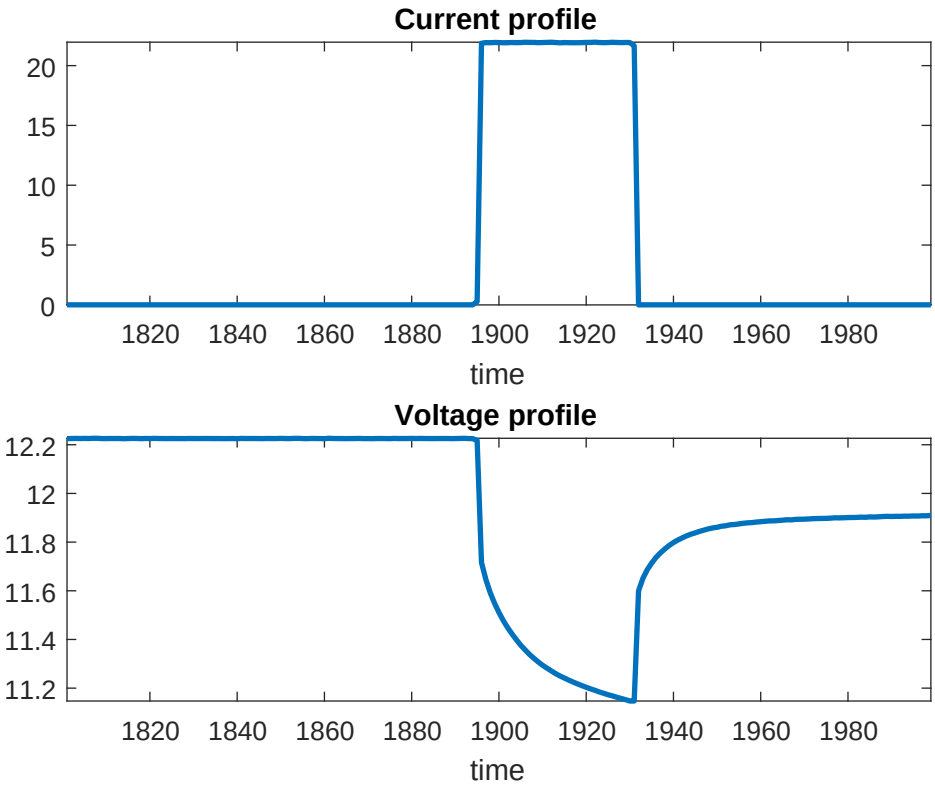

Figure 5.2. Volatge - current relationship

SOC	R_0	R_1	C_1	OCV
100%	0.0204	0.0111	738.328	12.479
90%	0.0204	0.0145	583.029	12.220
80%	0.0233	0.0120	723.552	11.931
70%	0.0236	0.0108	789.348	11.755
60%	0.0239	0.0105	843.271	11.589

Table 5.1. Model parameters at different SOC

5.2.2 State estimation using Kalman filter with varying model parameters

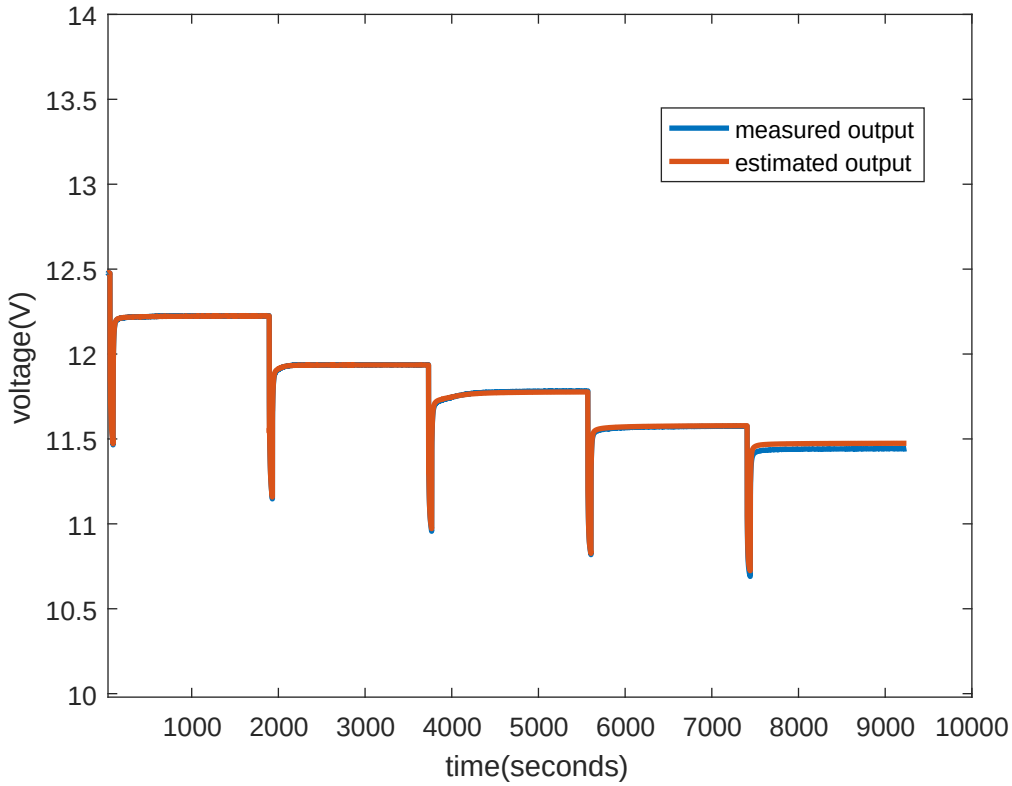

Figure 5.3. Dynamic estimator

Figure 5.3 illustrates the output voltage estimation for a system where the Kalman filter uses the model parameters corresponding to the SOC values to update the system at each discharge pulse. As a result, the estimated output closely follows the actual measured output. This can be used for anomaly detection, SOC and SOH estimation at the end of the test procedure but cannot be used for on-board estimation of model parameters for an active battery. For this purpose an adaptive estimation algorithm is required to adapt to the changing SOC during charge or discharge cycles and estimate the model parameters. This is explained in the following section.

5.3 Adaptive Estimation Algorithm

5.3.1 On-board parameter estimation

The battery management systems is responsible for controlling several parameters and two important parameters are the state of charge (SOC) and state of health (SOH). This requires the estimation of SOC and SOH to prevent failure and to maintain the lifetime of the battery. These two measures are determined using OCV and model parameters like resistance. For real-time estimation of SOC and SOH, an on-board or on-line estimation of the parameters and OCV is necessary. For this purpose, an adaptive estimation algorithm based on the least mean squares method is developed for the RC equivalent model of the Li-ion battery.

5.3.2 Adaptive algorithm

From section 3.4 the state space representation of the Li-ion battery is given by:

$$\begin{cases} \dot{v_c}(t) = \dfrac{-1}{R_t C_t} v_c(t) + \dfrac{1}{C_t} i(t) \\ v_{cell}(t) = OCV(SOC(t)) - i(t)R_s - v_c(t) \end{cases} \tag{5.14}$$

As the voltage across the RC branch v_c can neither be measured nor estimated, it is desirable to eliminate v_c for easier computation of the algorithm. The dependence of OCV on SOC expressed as $OCV(SOC)$ is represented as V_{oc} in the following section. The continuous-time differential of the terminal voltage can be expressed as:

$$\dot{v}_{cell} = V_{oc} - iR_s - \dot{v}_c \tag{5.15}$$

Substituting $\dot{v}_c$ in the output equation, the terminal voltage of the battery v_{cell} can be expressed in terms of the model parameters as follows:

$$\dot{v}_{cell} = -\frac{1}{R_t C_t} v_{cell} - R_s \dot{i} - \frac{R_t + R_s}{R_t C_t} i + \frac{V_{oc}}{R_t C_t} \tag{5.16}$$

This equation represents the reinterpretation of the dynamics of the battery in terms of v_{cell}. As the the model parameters are linearly dependent on the terminal voltage, it is possible to employ an adaptive estimation algorithm to determine the model parameters at each time step before the tracking error approaches zero. (Chiang et al., 2011). 5.16 can be expressed in terms of vectors as follows:

$$\dot{v}_{cell} = \theta^T X \tag{5.17}$$

where

$$\theta^T = [\theta_1 \quad \theta_2 \quad \theta_3 \quad \theta_4]^T = \begin{bmatrix} R_s & \dfrac{R_t + R_s}{R_t C_t} & \dfrac{1}{R_t C_t} & \dfrac{V_{oc}}{R_t C_t} \end{bmatrix} \tag{5.18}$$

$$X^T = [-\dot{i} \quad -i \quad -v_{cell} \quad 1] \tag{5.19}$$

The estimated output $\hat{v}_{cell}$ is given by:

$$\hat{\dot{v}}_{cell} = \hat{\theta}^T \hat{X} \tag{5.20}$$

where

$$\hat{\theta}^T = [\hat{\theta}_1 \quad \hat{\theta}_2 \quad \hat{\theta}_3 \quad \hat{\theta}_4]^T = \begin{bmatrix} \hat{R}_s & \widehat{\dfrac{R_t + R_s}{R_t C_t}} & \widehat{\dfrac{1}{R_t C_t}} & \widehat{\dfrac{V_{oc}}{R_t C_t}} \end{bmatrix} \tag{5.21}$$

$$\hat{X}^T = [-\hat{\dot{i}} \quad -\hat{i} \quad -\hat{v}_{cell} \quad 1] \tag{5.22}$$

By discretizing the system, the estimation error can be formed as:

$$e = v_{cell}[k] - \hat{v}_{cell}[k] \tag{5.23}$$

For the convergence of the estimated parameters, the error has to be driven to zero $\lim_{t\to\infty} e = 0$, and this can be achieved by different adaptive estimation algorithms. One such adaptive estimation algorithm is by using least mean squares method (Chaoui and Mandalapu, 2017).

The discrete-time representation of the output voltage is as follows:

$$v_{cell}[k] = \big(R_s e^{\left(\frac{-\Delta t}{R_t C_t}\right)} - R_t\big(1 - e^{\left(\frac{-\Delta t}{R_t C_t}\right)}\big)\big) i[k-1] - R_s i[k] + e^{\left(\frac{-\Delta t}{R_t C_t}\right)} v_{cell}[k-1] + \big(1 - e^{\left(\frac{-\Delta t}{R_t C_t}\right)}\big) V_{oc} \tag{5.24}$$

where

$$\theta = \begin{pmatrix} \hat{\theta}_1 \\ \hat{\theta}_2 \\ \hat{\theta}_3 \\ \hat{\theta}_4 \end{pmatrix} = \begin{pmatrix} \big(R_s e^{\left(\frac{-\Delta t}{R_t C_t}\right)} - R_t\big(1 - e^{\left(\frac{-\Delta t}{R_t C_t}\right)}\big)\big) \\ R_s \\ e^{\left(\frac{-\Delta t}{R_t C_t}\right)} \\ \big(1 - e^{\left(\frac{-\Delta t}{R_t C_t}\right)}\big) V_{oc} \end{pmatrix} \quad \text{and} \quad X = \begin{pmatrix} -i[k-1] \\ -i[k] \\ v[k-1] \\ 1 \end{pmatrix} \tag{5.25}$$

5.3.3 Least Mean Square Method

Least mean square is a stochastic gradient method and the signal statistics are estimated continuously. Hence, it is an adaptive filter. The algorithm iterates to minimize the estimation error and determines the model parameters. It can be described as follows:

$$\Delta\hat{\theta}(k) = \mu X(k) e(k) \tag{5.26}$$

After computing the vector parameter update (5.26), the vector parameters are updated using:

$$\hat{\theta}(k) = \hat{\theta}(k-1) + \Delta\hat{\theta}(k) \tag{5.27}$$

The parameters are updated until the error reaches zero. After $\hat{\theta}$ has converged sufficiently well, the parameters are evaluated. The convergence depends on the adaptive gain μ, although exact convergence results have not been formalized for this method. The adaptive

gain can be optimized to achieve the desired result. The battery model parameters can be evaluated as follows:

$$\begin{pmatrix} \hat{R}_s \\ \hat{R}_t \\ \hat{V}_{oc} \end{pmatrix} = \begin{pmatrix} \hat{\theta}_2 \\ \frac{\hat{\theta}_2\hat{\theta}_3 - \hat{\theta}_1}{1-\hat{\theta}_3} \\ \frac{\hat{\theta}_4}{1-\hat{\theta}_3} \end{pmatrix} \tag{5.28}$$

With the on-board estimation of the model parameters, the internal dynamics of the system can be estimated using the Kalman filter. Also, the estimation of the resistance and OCV is used to determine the SOC and SOH parameters.

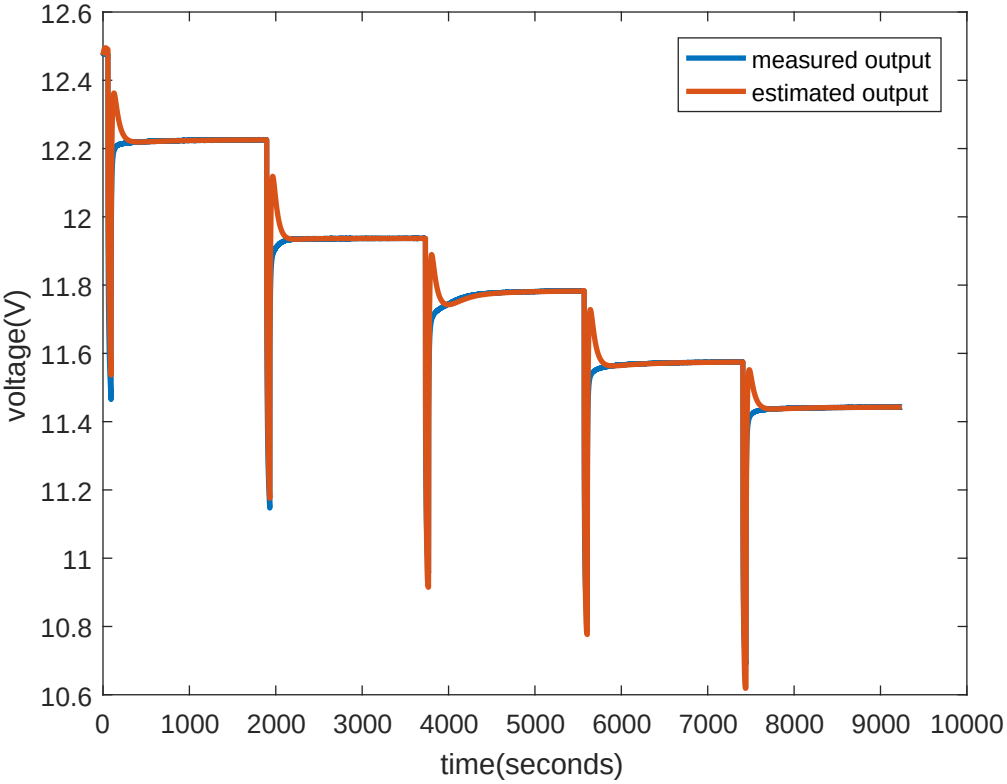

Figure 5.4. Adaptive estimator

The below Figure 5.4 illustrates the mRPT where the output voltage is estimated by the Kalman filter using the model parameters estimated by the adaptive estimation algorithm.

The steady state voltage variation at the end of the discharge pulse is related to the slower convergence of the model parameters which is influenced by the adaptive gain μ. Large values of the adaptive gain would lead to high fluctuations in the parameter estimation and small values take longer time for convergence of parameters. Optimal selection of the adaptive gain values is necessary for efficient parameter estimation and resulting state and output estimation. The fast discharge characteristics of the mRPT test make it a difficult use case for adaptive estimation. For this reason we do not use the adaptive method, but it may be more useful in standard drive cycle data (future work).

CHAPTER 6

ANOMALY DETECTION

To maintain the security of the battery systems, control methods are built to detect and react against attacks. In the case of stealthy attacks where the operators do not realize the attack, it is important to characterize the impact the attacker can have on the control process. Although there are several methods to detect the attacks, proper tuning is required to determine the performance of the detector and the capabilities of the attacker. In this research work we consider two types of detectors: static detectors and dynamic detectors.

6.1 Residual

In a dynamical system, faults and attacks can be generalized to be an anomaly which indicates the deviation of measurements from the estimated state. Fault/attack detection with the estimator uses the residuals which is the difference between what is measured and estimated. If the residual is larger than expected (larger than a predetermined threshold), there might be a fault/attack in the system.

The residual sequence r_k is defined as

$$r_k := \bar{y}_k - C\hat{x}_k = Ce_k + \eta_k + \delta_k, \tag{6.1}$$

where e_k is the estimation error. It is given by

$$e_k = x_k - \hat{x}_k \tag{6.2}$$

Then the residual evolves according to

$$\begin{cases} e_{k+1} = \big(F - LC\big)e_k - L\eta_k + w_k - L\delta_k, \\ \quad r_k = Ce_k + \eta_k + \delta_k. \end{cases} \tag{6.3}$$

6.2 Detection Procedures

There are several detection procedures for attack detection. In this thesis we focus on the detection procedures based on the distance measure. It uses a quadratic form of the residual to test for substantial variations in the covariance and expected value of the error between the observed and estimated outputs. This has several advantages over the arguably simplest detector that simply compares the absolute error to a threshold. Beyond testing for changes in the spread of the residual distribution, it provides an analytically tractable distribution. We consider both static and dynamic detectors. Various parameters are used to tune and maintain the performance of the detectors. In addition to the existing static chi-squared and CUSUM detectors, in this thesis, we focus on the windowed chi-squared detector and we have studied its performance to tune it for worst-case attack detection.

6.2.1 Windowed Chi-Squared Detector

The static chi-squared detector is one of the simplest and popular detector. But the CUSUM detector has some advantages because of its dynamic capabilities. However, its tuning requires both bias b and threshold τ values to be selected appropriately. If the bias is too small, the CUSUM test sequence becomes too large and if the bias is too large, the effect of the attacker might be lost or hidden and it provides more opportunity for sensor attacks to influence the system while still remaining undetected. So, a more of a middle-ground approach for dynamic attack detection is the windowed chi-squared detector. It has the advantages of a dynamic detector and involves the threshold and window length to be chosen. If

$$w_k = \sum_{i=k-\ell+1}^{k} z_i = \sum_{i=k-\ell+1}^{k} r_i^T \Sigma^{-1} r_i, \quad \widetilde{k} = k \tag{6.4}$$

Design parameter: threshold $\beta \in \mathbb{R}_{>0}$ and $\ell \in \mathbb{N}$

Output: alarm time(s) $\widetilde{k}$

This considers the moving sum of z_i over a sliding window $[k-\ell+1; k]$ of length ℓ, where z_i are independent chi-squared variables each with m degree of freedom, and w_k is the sum of ℓ independent chi-squared variables.

The additivity property of chi-squared distribution states that: the sum of two independent chi-squared variables with m and n degrees of freedom, respectively, is a chi-squared variable with $m+n$ degrees of freedom. It follows from the additivity property that the sum of independent chi-squared variables is also chi-square distributed. So, w_k is chi-square distributed with ℓp degrees of freedom.

The occurrence of an alarm in a detector when there are no attacks to the systems is referred to as a false alarm. It is denoted by $\mathcal{A}$. The threshold β of the windowed chi-squared detector is determined according to the following theorem.

Theorem 1. *Assume that there are no attacks to the system and consider the windowed chi-squared detector with threshold $\beta \in \mathbb{R}_{>0}$ and $r_k \sim \mathcal{N}(0, \Sigma)$. Let $\beta = \beta^* := 2P^{-1}(1-\mathcal{A}^*, \frac{p\ell}{2})$, where $P^{-1}(\cdot,\cdot)$ denotes the inverse regularized lower incomplete gamma function, then $\mathcal{A} = \mathcal{A}^*$.*

Proof: By construction, for all $i \in \mathbb{N}$, z_i are independent chi-squared variables with p degrees of freedom. Thus, w_k is the sum of ℓ independent chi-squared variables. The sum of two independent chi-squared variables with p and q degrees of freedom, respectively, is a chi-squared variable with $p+q$ degrees of freedom (Lancaster, 1969). Hence, the windowed chi-squared statistic w_k falls according to a chi-squared distribution with $p\ell$ degrees of freedom. The cumulative distribution function is then given by $\mathcal{F}(w) = P(\frac{p\ell}{2}, \frac{w}{2})$, where $P(\cdot,\cdot)$ is the regularized lower incomplete gamma function. The false alarm rate is simply the portion of

the w_k distribution that falls in the tail beyond the threshold β

$$\mathcal{A} = \text{pr}(w_k > \beta) = 1 - \mathcal{F}(\beta) = 1 - P\left(\frac{p\ell}{2}, \frac{\beta}{2}\right). \tag{6.5}$$

Inverting this relationship to solve for β yields the result. □

Solving for β:

$$\begin{cases} \mathcal{A} = 1 - P\left(\frac{p\ell}{2}, \frac{w}{2}\right) \\ P\left(\frac{p\ell}{2}, \frac{w}{2}\right) = 1 - \mathcal{A} \\ \frac{w}{2} = P^{-1}\left(1 - \mathcal{A}^*, \frac{p\ell}{2}\right) \end{cases} \tag{6.6}$$

With no attacks,

$$w = w_k \to \beta = \beta^* = 2P^{-1}\left(1 - \mathcal{A}^*, \frac{p\ell}{2}\right) \tag{6.7}$$

□

6.2.2 Static Chi-Squared Detector

Chi-squared procedure uses a quadratic form to test for substantial variations in the covariance of the error between the observed state and the estimated state.

If

$$z_k = r_k^T \Sigma^{-1} r_k > \alpha, \quad \widetilde{k} = k \tag{6.8}$$

Design parameter: threshold $\alpha \in \mathbb{R}_{>0}$

Output: alarm time(s) $\widetilde{k}$

The quadratic expression $r_k^T \Sigma^{-1} r_k$ represents the distance measure which follows chi-squared distribution.

$$\begin{cases} E[z_k] = p \\ var[z_k] = 2p \end{cases} \tag{6.9}$$

$r_k \sim \mathcal{N}(0, \Sigma)$, z_k follows a chi-squared distribution with p degrees of freedom. Similar to the determination of the threshold for windowed chi-squared detector, the threshold α of the static chi-squared detector can be determined according to the following theorem.

Lemma 1. *(Murguia and Ruths, 2016b). Assume that there are no attacks to the system i.e.* $\delta_k = 0$ *and consider chi-squared detector, with threshold* $\alpha \in \mathbb{R}_{>0}$, $r_k \sim N(0, \Sigma)$. *Let* $\alpha = \alpha^* := 2P^{-1}(1 - \mathcal{A}^*, \frac{p}{2})$, *where* $P^{-1}(\cdot, \cdot)$ *denotes the inverse regularized lower incomplete gamma function, then* $\mathcal{A} = \mathcal{A}^*$.

6.2.3 CUSUM detector

CUSUM (Cumulative Sum) is a sequential analysis technique which is used to aggregate the error over an adaptive window to protect the system against small, but persistent, attacks. Given a chosen distance measure z_k (considering the quadratic distance measure $z_k = r_k^T \Sigma^{-1} r_k$). Once S_k exceeds the threshold τ or becomes negative, the test is reset to zero.

$$\begin{cases} S_1 = 0, \\ S_k = \max(0, S_{k-1} + z_k - b), \quad \text{if} \quad S_{k-1} \leq \tau, \\ S_k = 0 \quad \text{and} \quad \widetilde{k} = k - 1, \quad \text{if} \quad S_{k-1} \leq \tau, \end{cases} \tag{6.10}$$

Design parameters: bias $b \in \mathbb{R}_{>0}$ and threshold $\tau \in \mathbb{R}_{>0}$

Design: alarm time(s) $\widetilde{k}$

6.3 Feedback Controller

A closed loop system is required to understand the effect of the attack on the state of the system. This helps the operators to assess the impact of the attack and to take appropriate

defensive measures to maintain the performance of the system. Consider an output feedback controller of the form:

$$u_k := K\hat{x}_k \tag{6.11}$$

where u_k is the control input, $K \in \mathbb{R}^{m\times n}$ is the feedback control matrix, $\hat{x}_k \in \mathbb{R}^n$ is the state of Kalman filter. It is assumed that (F, G) is stabilizable.

Given the estimation error e_k, the closed-loop system becomes:

$$\begin{cases} x_{k+1} = (F + GK)x_k + GKe_k + w_k, \\ e_{k+1} = (F - LC)e_k - L\delta_k - L\eta_k + w_k. \end{cases} \tag{6.12}$$

It can be observed that the estimation error dynamics is directly affected by the attack sequence. Whereas, the system dynamics is indirectly affected through the feedback interconnection term GKe_k.

6.4 Zero Alarm Attacks

Zero Alarm Attacks or Stealthy Attacks are those which stay undetected by the detectors. It is assumed that the attacker has real-time access to the sensor measurements, system dynamics, Kalman Filter, control inputs and the detection procedures (Murguia and Ruths, 2016a). It is able to inject false measurements in the sensor measurements and stays undetected (Qadeer et al., 2017). Such attacks are useful for the system design because it allows the operator to understand the extent of damage the attacker can cause if the attacker chooses to remain below the threshold.

To understand the impact of the attacker on the windowed chi-squared detector, the zero alarm attack sequence is formulated. The attack sequence for zero alarm attack is such that the test saturates and is maintained at the detection threshold. For the windowed

chi-squared detector the attack sequence δ is designed such that the windowed chi-squared statistic w_k is maintained at threshold β so that it can stealthily impact the system without raising the alarm.

We first motivate this approach by studying the static chi-squared detector. Let us assume a vector $\bar{\alpha} \in \mathbb{R}^p$ such that $\bar{\alpha}^T \bar{\alpha} = \alpha$. Then the attack sequence is defined as:

$$\delta_k = C\hat{x}_k - y_k + \Sigma^{\frac{1}{2}}\bar{\alpha} = -Ce_k - \eta_k + \Sigma^{\frac{1}{2}}\bar{\alpha}, \tag{6.13}$$

Here the attack sequence is assumed to have access to the output y_k or it alters the sensor measurement. So, the distance measure becomes:

$$\begin{cases} z_k = r_k^T \Sigma^{-1} r_k \\ z_k = (Ce_k + \eta_k + \delta_k)^T \Sigma^{-1} (Ce_k + \eta_k + \delta_k) \\ z_k = \alpha \end{cases} \tag{6.14}$$

Here the distance measure equals the threshold α and it does not exceed the threshold, the process does not raise alarms.

Similar to (6.14), the definition of the windowed chi-squared statistic is given by:

$$w_k = \sum_{i=k-\ell+1}^{k} (Ce_i + \eta_i + \delta_i)^T \Sigma^{-1} (Ce_i + \eta_i + \delta_i). \tag{6.15}$$

To saturate $w_k = \beta$, the attack sequence on each individual chi-squared distribution z_k is given by:

$$\delta_i = -Ce_i - \eta_i + \Sigma^{\frac{1}{2}}\bar{\delta}_i \tag{6.16}$$

We know that the windowed chi-squared detector is summed over the time window of length ℓ, hence it is possible to design an infinite array of different $\bar{\delta}_k$ profiles which sums up to β

$$w_k = \sum_{i=k-\ell+1}^{k} \bar{\delta}_i^T \bar{\delta}_i = \beta \tag{6.17}$$

For example the following time-varying attack sequence satisfies $w_k = \beta$:

$$\bar{\delta}_k = \begin{cases} \bar{\beta}, & (k - k^*) \bmod \ell = 0, \\ 0, & \text{otherwise}, \end{cases} \tag{6.18}$$

where

$$\bar{\beta} := \left\{ \bar{\beta} \in \mathbb{R}^p | \bar{\beta}^T \bar{\beta} = \beta \right\}. \tag{6.19}$$

Although windowed chi-squared detector implements an attack that is time-varying, static chi-squared detector and CUSUM implements an attack that does not vary with time. To make an equitable comparison of all the three detectors, we select a static sequence:

$$\bar{\delta}_k = \bar{\delta} = \frac{\bar{\beta}}{\ell}, \tag{6.20}$$

Hence, for a windowed chi-squared detector, the estimation error dynamics (6.12) is obtained by substituting the attack sequence (6.16):

$$\begin{cases} e_{k+1} = (F - LC)e_k - L\delta_k - L\eta_k + w_k, \\ e_{k+1} = (F - LC)e_k - L(-Ce_i - \eta_i + \Sigma^{\frac{1}{2}}\bar{\delta}_i) - L\eta_k + w_k, \\ e_{k+1} = Fe_k - LCe_k + LCe_k + L\eta_i - L\Sigma^{\frac{1}{2}}\bar{\delta}_i - L\eta_k + w_k, \\ e_{k+1} = Fe_k - L\Sigma^{\frac{1}{2}}\dfrac{\bar{\beta}}{\ell} - L\eta_k + w_k. \end{cases} \tag{6.21}$$

The closed-loop system dynamics is given by:

$$\begin{cases} x_{k+1} = (F + GK)x_k + GKe_k + w_k, \\ e_{k+1} = Fe_k - L\Sigma^{\frac{1}{2}}\dfrac{\bar{\beta}}{\ell} - L\eta_k + w_k. \end{cases} \tag{6.22}$$

Theorem 2. *Consider the windowed chi-squared detector and let the sensors be attacked by the zero-alarm attack sequence* (6.20). *If* $\rho[F] < 1$, *then* $\lim_{k\to\infty} \|E[x_k]\| = \gamma^{\ell}_{\chi^2}$, *where*

$$\gamma^{\ell}_{\chi^2} := \left\| (I - F - GK)^{-1} GK (I - F)^{-1} L \Sigma^{\frac{1}{2}} \frac{\bar{\beta}}{\ell} \right\|, \tag{6.23}$$

and $\bar{\beta}$ *as defined in* (6.19).

Proof: By construction and assumption, $\rho[F + GK] < 1$ and $\rho[F] < 1$. This implies that $(I - F - GK)$ and $(I - F)$ are invertible, respectively; hence, system (6.22) has a unique equilibrium, in expectation, given by

$$\begin{cases} E[x_k] = \bar{x} := (I - F - GK)^{-1} GK (I - F)^{-1} L \Sigma^{\frac{1}{2}} \bar{\delta}, \\ E[e_k] = \bar{e} := (F - I)^{-1} L \Sigma^{\frac{1}{2}} \bar{\delta}. \end{cases}$$

Substituting (6.20) yields the matrix in $\gamma^{\ell}_{\chi^2}$. To ensure this equilibrium is attractive, we use (6.22) to show that the evolution of the differences $E[e_k] - \bar{e}$ and $E[x_k] - \bar{x}$ satisfy

$$\begin{aligned} E[x_{k+1}] - \bar{x} &= (F + GK)(E[x_k] - \bar{x}) - GK(E[e_k] - \bar{e}), \\ E[e_{k+1}] - \bar{e} &= F(E[e_k] - \bar{e}). \end{aligned}$$

Since $\rho[F + GK] < 1$ and $\rho[F] < 1$, the equilibrium $[\bar{x}, \bar{e}]^T$ is exponentially stable, i.e., $\lim_{k\to\infty} E[e_k] = \bar{e}$ and $\lim_{k\to\infty} E[x_k] = \bar{x}$. The Euclidean norm on $\mathbb{R}^n$ is a continuous function from $\mathbb{R}^n$ to $\mathbb{R}_{\geq 0}$ It follows that $\lim_{k\to\infty} \|E[x_k]\| = \| \lim_{k\to\infty} E[x_k]\| = \|\bar{x}\|$. □

Similarly, the steady state deviation of static chi-squared and CUSUM detectors can be determined. It is explained in the following results.

Lemma 2. *(Murguia and Ruths, 2016b). Consider the chi-square detector and let the sensors be attacked by the chi-squared zero-alarm attack sequence* (6.13). *If* $\rho[F] < 1$, *where* $\rho[\cdot]$ *denotes spectral radius, then* $\lim_{k\to\infty} \|E[x_k]\| = \gamma_{\chi^2}$, *where*

$$\gamma_{\chi^2} := \left\| (I - F - GK)^{-1} GK (I - F)^{-1} L \Sigma^{\frac{1}{2}} \bar{\alpha} \right\|. \tag{6.24}$$

Similarly, for the CUSUM detector, the zero-alarm attack sequence is given by

$$\delta_k = \begin{cases} -Ce_k - \eta_k + \Sigma^{1/2}\bar{\tau}, & k = k^*, \\ -Ce_k - \eta_k + \Sigma^{1/2}\bar{b}, & k > k^*, \end{cases} \tag{6.25}$$

where $\bar{b} \in \mathbb{R}^p$ (resp., $\bar{\tau} \in \mathbb{R}^p$) is any vector such that $\bar{b}^T\bar{b} = b$ (resp., $\bar{\tau}^T\bar{\tau} = \tau$) and k^* is the starting attack instant. The first step of this attack sequence saturates the test statistic $S_k = \tau$ and the subsequent steps maintain the statistic at the threshold.

Lemma 3. *(Murguia and Ruths, 2016b). Consider the CUSUM detector and let the sensors be attacked by the CUSUM zero alarm attack sequence* (6.25)*. If* $\rho[F] < 1$*, then* $\lim_{k\to\infty} \|E[x_k]\| = \gamma_{CS}$*, where*

$$\gamma_{CS} := \left\| (I - F - GK)^{-1} GK (I - F)^{-1} L \Sigma^{\frac{1}{2}} \bar{b} \right\|. \tag{6.26}$$

6.5 Detector Comparison

For stealthy attacks, the derivation of upper bounds on the steady state value of the expectation of the state deviation ($\|E[x_k]\|$) considering $\rho[F] < 1$, help in comparing the different types of detectors. The thresholds of the three detectors $\bar{\alpha}$, $\bar{b}$ and $\bar{\beta}$ indicates that the asymptotic bounds γ_{χ^2}, γ_{CS}, and $\gamma^{\ell}_{\chi^2}$ are different only due to the differing values of $\sqrt{\alpha}$, $\sqrt{b}$, and $\sqrt{\beta}/\ell$.

6.5.1 Comparison between Static Chi-Square and CUSUM detectors

To make an equitable comparison between static chi-square and CUSUM, let $\widetilde{b} = c\bar{\alpha}$ for some $c \in \mathbb{R}$. By construction $\widetilde{b} = c\bar{\alpha} \rightarrow \widetilde{b}^T\widetilde{b} = b = c^2\bar{\alpha}^T\bar{\alpha} = c^2\alpha$, hence $c = \pm\sqrt{b/\alpha}$.

$\mathcal{A}^*$ is selected to be a small value so that there are only a few false alarms in the attack free case and the bias b is selected close to the degree of the system to increase the chance

of attack detection. So, let us consider the false alarms to be between 1% and 10% i.e. $\mathcal{A}^* \in [0.01, 0.1]$ and let $b = 2$. According to Lemma 1 the threshold is calculated using the equation $\alpha^* = 2P^{-1}\left(1 - \mathcal{A}^*, \frac{p}{2}\right)$, then $\alpha \in [9.21, 4.60]$. With $b \approx \bar{b} = p = 2, 0.45 < |c| < 0.65$. Hence $|c| < 1$ which implies $b < (\alpha)$. This implies that for the same class of attacks and $\mathcal{A}^* \to [0.01, 0.1]$, the static chi-squared procedure leads to at least two times larger upper bounds than CUSUM.

6.5.2 Comparison between CUSUM and the Windowed Chi-Square detector

To make an equitable comparison between windowed chi-square and CUSUM, let $\widetilde{b} = c(\bar{\alpha}/\ell)$ for some $c \in \mathbb{R}$. By construction,

$\widetilde{b} = c(\bar{\alpha}/\ell) \to \widetilde{b}^T\widetilde{b} = b = c^2\bar{\alpha}^T\bar{\alpha}/\ell = c^2(\alpha/\ell)$, hence $c = \pm\sqrt{b\ell/\alpha}$

$\mathcal{A}^*$ is selected to be a small value so that there are only a few false alarms. Let false alarms be between 1% and 10% i.e. $\mathcal{A}^* \in [0.01, 0.1]$ and $p = 2$ which implies two dimensional outputs. For the length of the window $\ell = 5$,the threshold $\alpha^* = 2P^{-1}(1 - \mathcal{A}^*, \frac{p\ell}{2}) \in [23.20, 15.98]$. The value of b is chosen as close as possible to p so that the chances of attack detection increases. With $b \approx \bar{b} = p = 2$, $0.65 < |c| < 0.79$. Hence $|c| < 1$ which implies $b < (\beta/\ell)$. Therefore, the windowed chi-squared procedure leads to larger upper bounds than the CUSUM.

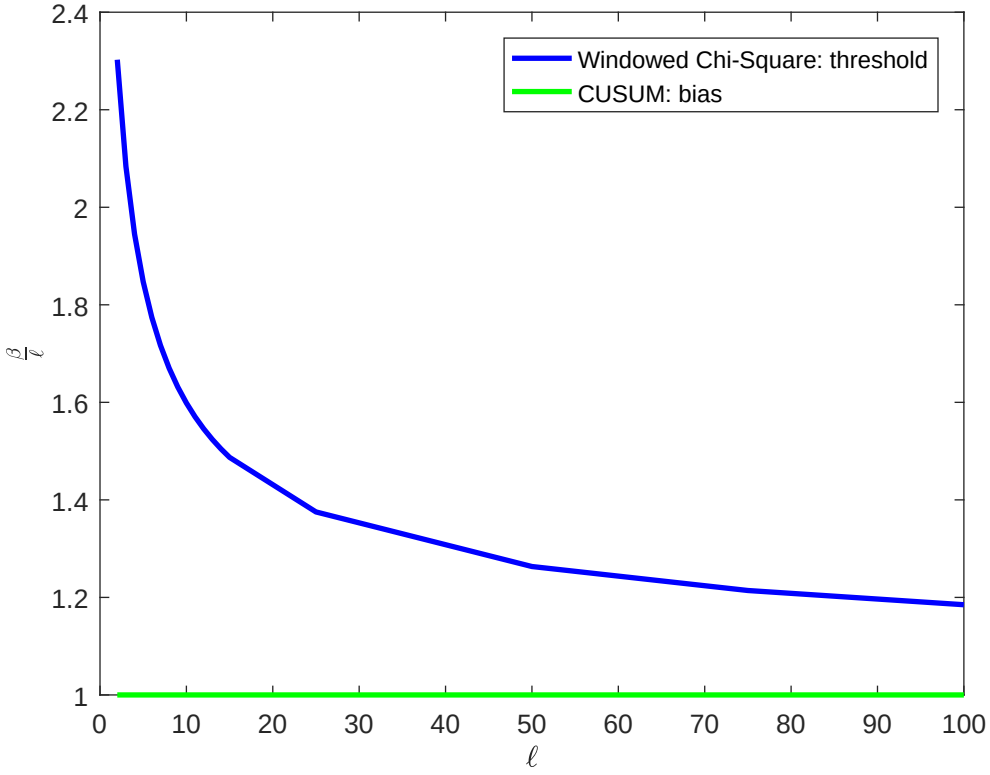

Figure 6.1. Comparison between CUSUM and the Windowed Chi-Squared Detector for increasing window lengths

From the Figure 6.1 it can be inferred that the threshold of the windowed chi-squared detector reduces with the increasing window length. This results in the reduction of the state deviation and upper bounds thus reducing the impact the attack can have on the system.

6.5.3 Performance of Static Chi-Squared Detector

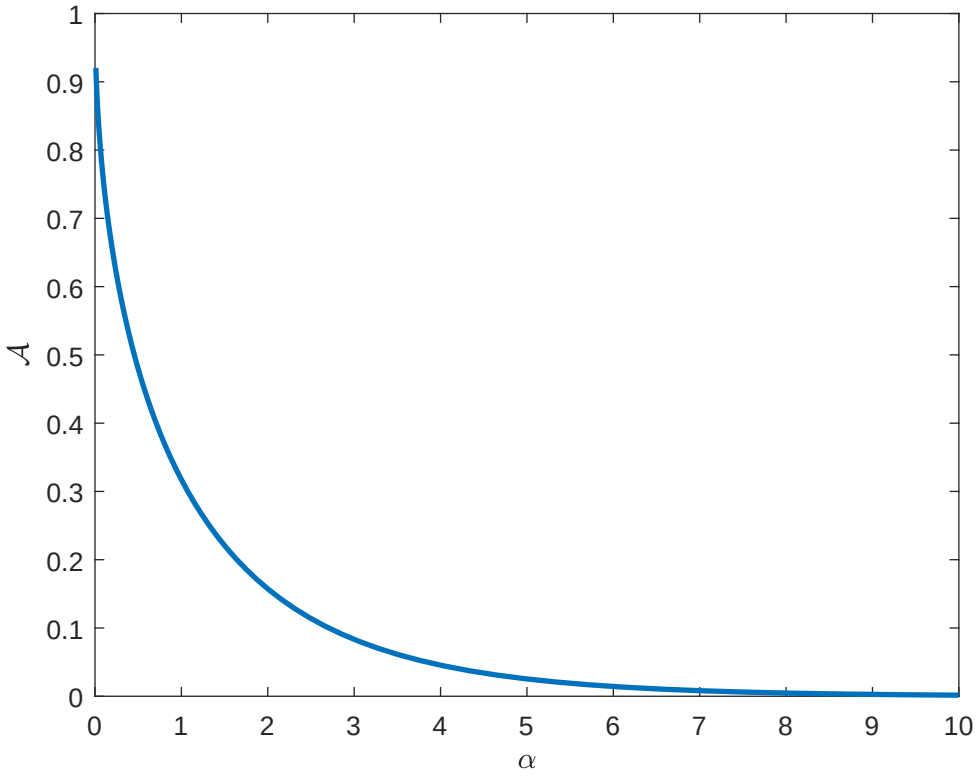

Figure 6.2. Performance of the Static Chi-Squared Detector

Figure 6.2 illustrates that for a static chi-squared detector, the threshold is less for higher false alarm rates. This implies that the steady state deviation is low for higher false alarm rates.

6.5.4 Performance of the Windowed Chi-Squared Detector

Analysis of the performance of the windowed chi-squared detector is necessary to understand the trade-offs between various parameters involved in tuning the detector and in achieving better performance.

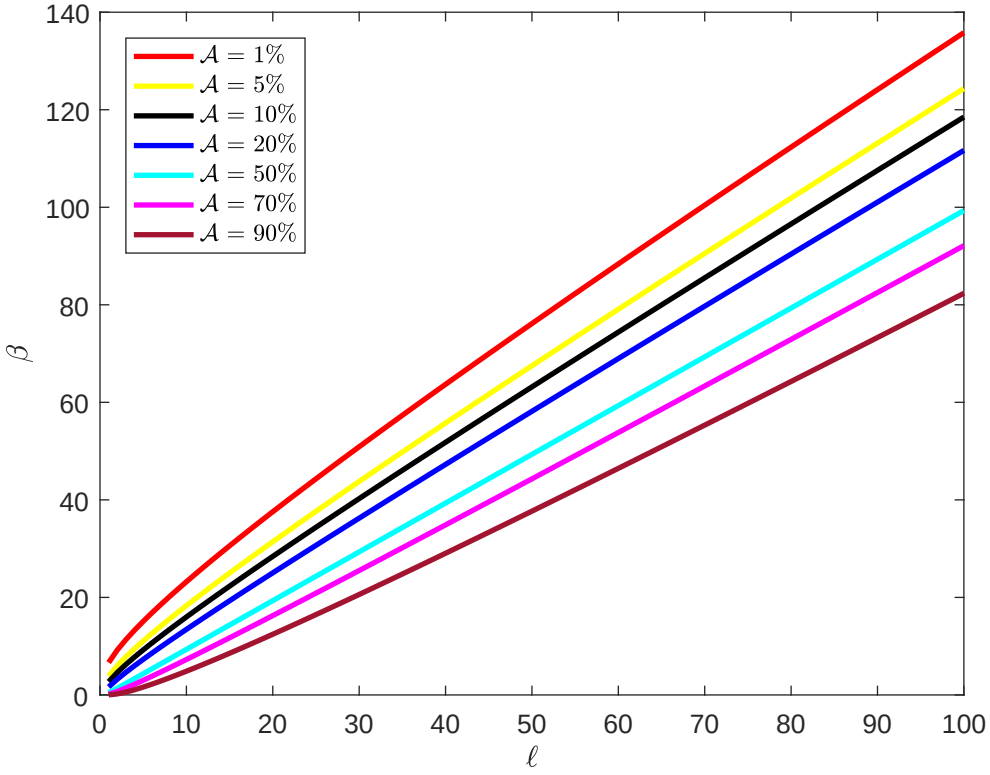

Figure 6.3. Threshold (β) v/s Window Length (ℓ) for varying False Alarm Rates ($\mathcal{A}$)

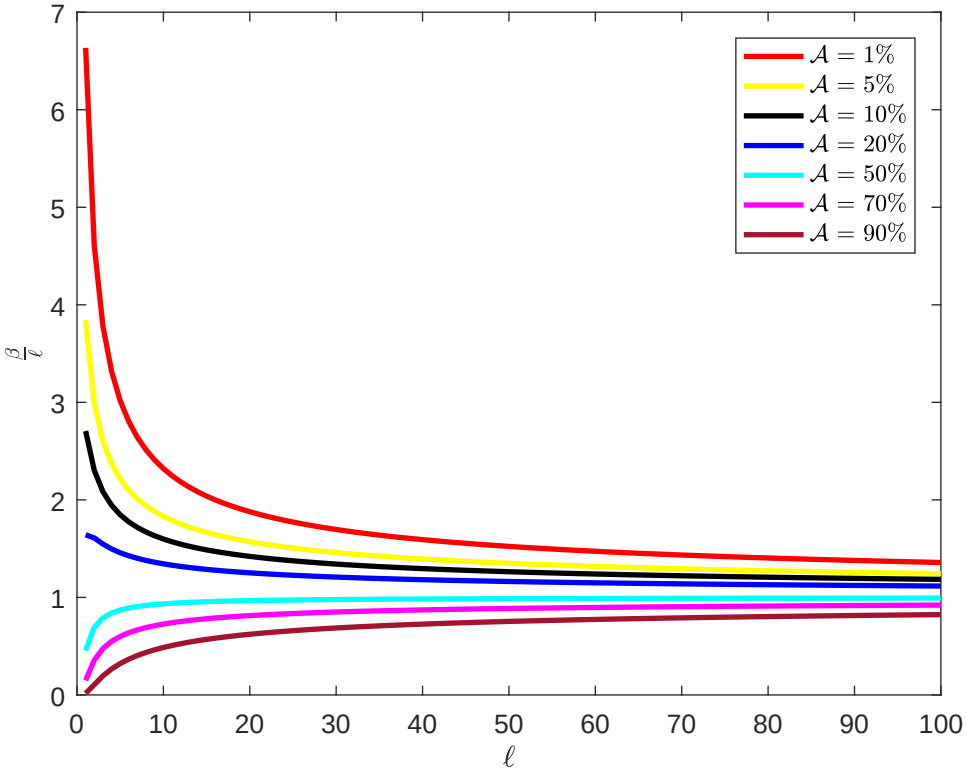

Figure 6.4. Threshold ($\frac{\beta}{\ell}$) v/s Window Length (ℓ) for varying False Alarm Rates ($\mathcal{A}$)

Figure 6.3 shows that threshold (β) is higher for lower false alarm rates ($\mathcal{A}$) and further increases with the increase in the window length (ℓ). However, Figure 6.4 shows that when the threshold is divided by the length (for equitable comparison) i.e. $\frac{\beta}{\ell}$, lower false alarm rates have higher values of $\frac{\beta}{\ell}$ and it reduces with the increase in the window length (ℓ).

From these results, we can understand that to limit the number of alarms in the attack free case, we have to select lower values of false alarm rates $\mathcal{A}$. In this context, $\alpha > b \approx p$. At the same time, $\beta/\ell < \alpha$. With these assumptions, we observe that: $\gamma_{\chi^2} > \gamma_{\text{CS}}$ and $\gamma_{\chi^2} > \gamma^{\ell}_{\chi^2}$. The windowed chi-squared detector performs an interesting function role and to better determine its performance against the CUSUM, we develop the following result.

Proposition 1. *Given a windowed chi-squared detector with window length ℓ and a CUSUM detector with bias tuned to $b = p$, the following is satisfied:*

$$\lim_{\ell \to \infty} \gamma_{\chi^2}^{\ell} = \gamma_{CS}, \tag{6.27}$$

where p is the dimension of the measurement vector.

Proof: The central limit theorem provides the asymptotic properties of the sample average $S_\ell = \frac{1}{\ell}(X_1 + X_2 + \cdots + X_\ell)$, given a sequence of ℓ i.i.d. random variables, $X_1,\ X_2,\ \ldots,\ X_\ell$, each with expected value μ and finite variance σ^2. The central limit theorem states that $\sqrt{\ell}(S_\ell - \mu)$ converges in distribution to $N(0, \sigma^2)$ as ℓ approaches infinity.
Here, the windowed chi-squared procedure computes then the sum (not the average) of chi-squared random variables $X_k = z_k = r_k^T \Sigma^{-1} r_k$ with p degrees of freedom, since $r_k \sim N(0, \Sigma)$ and $r_k \in \mathbb{R}^p$. Since $X_k = z_k$ is chi-square distributed with p degrees of freedom, it has mean $\mu = p$ and variance $\sigma^2 = 2p$. Thus, by the central limit theorem, the sample average approaches $N(\mu, \frac{\sigma^2}{\ell}) = N(p, \frac{2p}{\ell})$. From this, the sum (not average) approaches $N(\ell\mu, \ell\sigma^2) = N(p\ell, 2p\ell)$.

Note that determining the threshold β to satisfy a false alarm rate $\mathcal{A}$ for the asymptotic sum distribution $N(p\ell, 2p\ell)$ is equivalent to identifying the threshold β/ℓ to satisfy the same false alarm rate for the asymptotic sample average distribution $N(p, \frac{2p}{\ell})$. Notice that the latter distribution approaches mean p with shrinking variance. In the limit, the variance goes to zero, which means the threshold (in fact the entire distribution) collapses down to the mean value p. Thus for large values of window length ℓ, the value of β/ℓ to satisfy a chosen false alarm rate (in fact *any* alarm rate) converges to p. Substituting $\beta/\ell \to p$ into $\gamma_{\chi^2}^{\ell}$ and substituting $b \approx p$ into γ_{CS} then yields the result. □

It is important to note that this result is system independent, and thus purely a comparison of the detectors in the limiting case. Considering the case when $p = 1$, in Figure 6.4, we show the nonlinear trade-offs between the selection of β and ℓ to maintain the same false alarm rate $\mathcal{A}$. This plot demonstrates the convergence of the distribution as $\ell \to \infty$ to be centered at $p = 1$ with diminishing variance.

6.5.5 Simulation Results

The fault detection problems are studied for a well stirred chemical reactor with heat exchanger. The system is used to demonstrate the results. The state input and output vectors of the considered reactor are:

$$x(t) := \begin{bmatrix} C_o \\ T_o \\ T_w \\ T_m \end{bmatrix} \quad u(t) := \begin{bmatrix} C_u \\ T_u \\ T_{w,u} \end{bmatrix} \quad y(t) := \begin{bmatrix} C_o \\ T_o \\ T_w \end{bmatrix} \tag{6.28}$$

where:

C_o : Concentration of the chemical product

T_o : Temperature of the product

T_w : Temperature of the jacket of water of heat exchanger

T_m : Coolant temperature

C_u : Inlet concentration of reactant

T_u : Inlet temperature

$T_{w,u}$: Coolant water inlet temperature

$$F = \begin{pmatrix} 0.0273 & 0 & 0 & 0 \\ 0 & 0.0268 & 0.0001 & 0.0068 \\ 0 & 0.0004 & 0 & 0.0018 \\ 0 & 0.0619 & 0.0055 & 0.2478 \end{pmatrix}, \quad G = \begin{pmatrix} 0.0271 & 0 & 0 \\ 0 & 0.2665 & 0.0001 \\ 0 & 0.0005 & 0.0276 \\ 0 & 0.0761 & 0.0114 \end{pmatrix}$$

$$L = \begin{pmatrix} 0.0033 & 0 & 0 \\ 0 & 0.0033 & 0 \\ 0 & 0 & 0 \\ 0 & 0.0147 & 101.3810 \end{pmatrix}, \quad R_2 = 100 \times I_3, \quad C = \begin{pmatrix} 1 & 0 & 0 & 0 \\ 0 & 1 & 0 & 0 \\ 0 & 0 & 1 & 0 \end{pmatrix}$$

$$K = \begin{pmatrix} 3.2856 & -0.7139 & -0.8301 & 1.4940 \\ -0.0244 & 5.0912 & 2.0507 & -3.6645 \\ 0.2707 & 54.5562 & 99.8275 & -117.5190 \end{pmatrix}, \quad R_1 = \begin{pmatrix} 13.8785 & 0 & 0 & 0 \\ 0 & 13.6531 & 0.0141 & 2.1122 \\ 0 & 0.0141 & 1.3808 & 0.2623 \\ 0 & 2.1122 & 2.623 & 34.1805 \end{pmatrix}.$$

Degradation of steady state due to stealthy attacks

Steady state degradation is used to quantify the effect of the attack sequence on the state of the system. Here, we characterize the steady state deviation of the expectation of the state because of the attack sequence, when the system dynamics and control strategy is known. The nonlinear model is linearized about the origin $x(t) = 0_{4\times1}$. When the detectors are deployed for attack detection and the attack sequence is given by the zero-alarm attacks, with,

$\bar{\alpha} = \sqrt{\frac{\alpha}{p}}\bar{\delta}$, $\tilde{b} = \sqrt{\frac{b}{p}}\bar{\delta}$, $\bar{\tau} = \sqrt{\frac{\tau+b-S_{k-1}}{p}}\bar{\delta}$, and $\bar{\delta} = 1_{p\times1}$.

For CUSUM $b = 2\bar{b} =$ and $\tau = \tau^* = 4.1002$ such that, $A = A^* = 0.02$. The attacks are induced at $k = 100$.

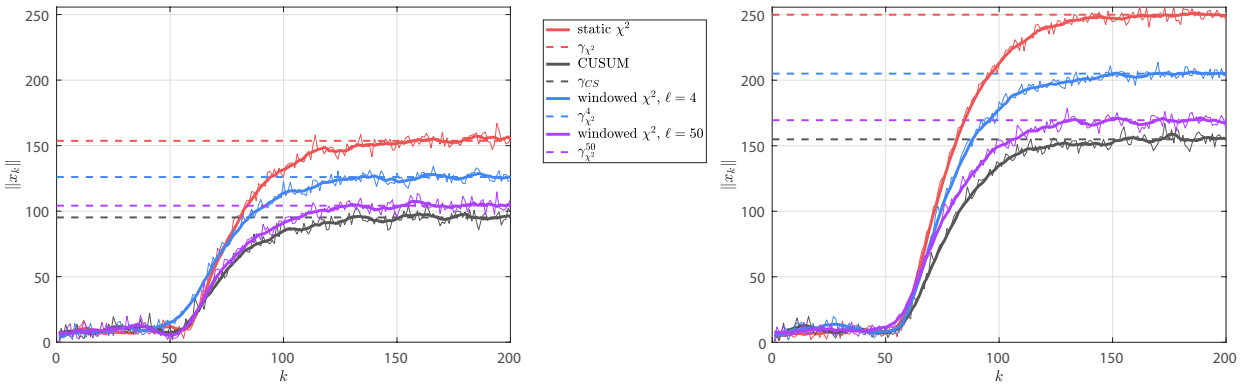

Figure 6.5. State degradation: Detector comparison

The theoretical results are validated on a model developed for a well stirred chemical reactor. Figure 6.5 shows the evolution of $||x_k||$ for the static chi-squared, CUSUM and windowed chi-squared detectors when they are deployed for detection with their respective attack sequences δ_k. The attack is induced at time step $k = 50$. The two plots represent the performance of the detectors for different attack sequences which vary by their threshold. The detectors are compared by their steady state deviation values. In both the plots we can observe that the steady state degradation for static chi-squared is the highest and that of CUSUM is the lowest, and the steady state degradation for windowed chi-squared decreases with the increase in window length and approximates to that of CUSUM.

CHAPTER 7

ANOMALY DETECTION IN BATTERIES

The distance measure plot is used to indicate the presence of an anomaly in the battery. Presence of anomaly is indicated when the distance measure z_k exceeds threshold. Using the estimated output from the Kalman filter (as explained in section (5.2)) the residual is determined. This residual is used to determine the distance measure (6.8) which also involves the covariance matrix Σ given by the equation (5.6). Σ is the covariance of the measurement noise η_k. The distance measure is calculated at every time step for the mini Reference Performance Test (mRPT) with five discharge pulses reducing the SOC by 10%. Here the system is designed for 1% false alarm rate ($\mathcal{A}$) i.e. one false alarm in 100 time steps does not indicate an anomaly.

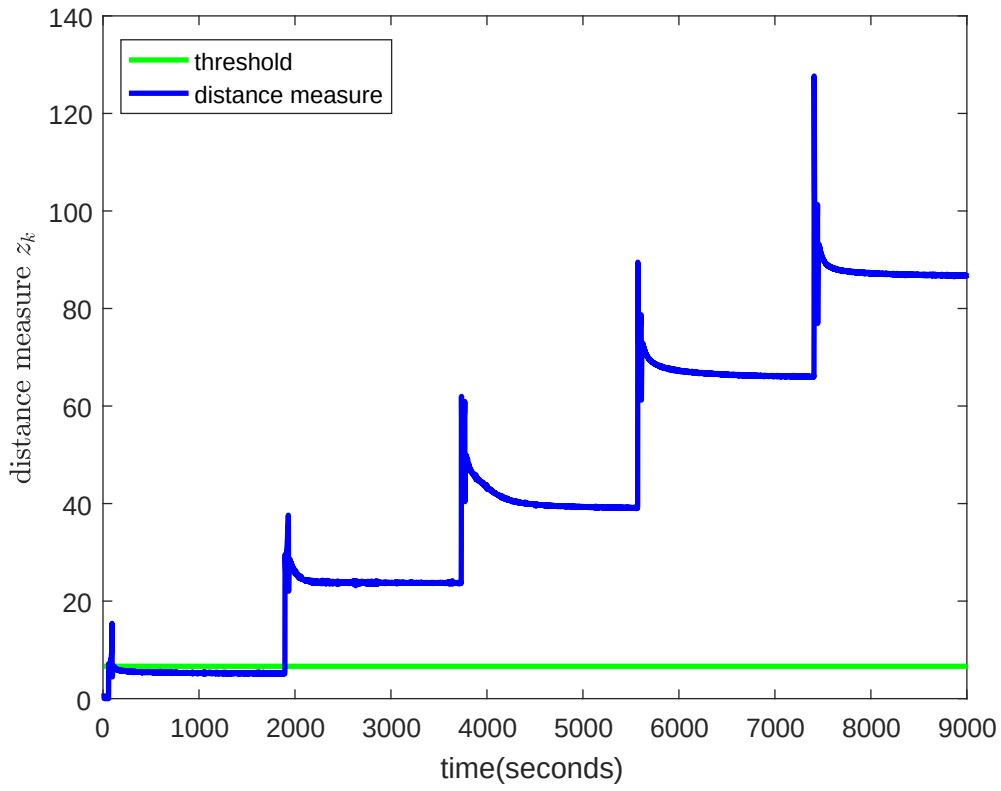

Figure 7.1. Distance measure of the static estimator.

Figure 7.1 illustrates the distance measure plot for the system with model parameters fixed at 100% SOC. The model parameters are not changing with the SOC but remain constant. This causes the distance measure to exceed the threshold at each time step. This does not accurately indicate the presence of an anomaly.

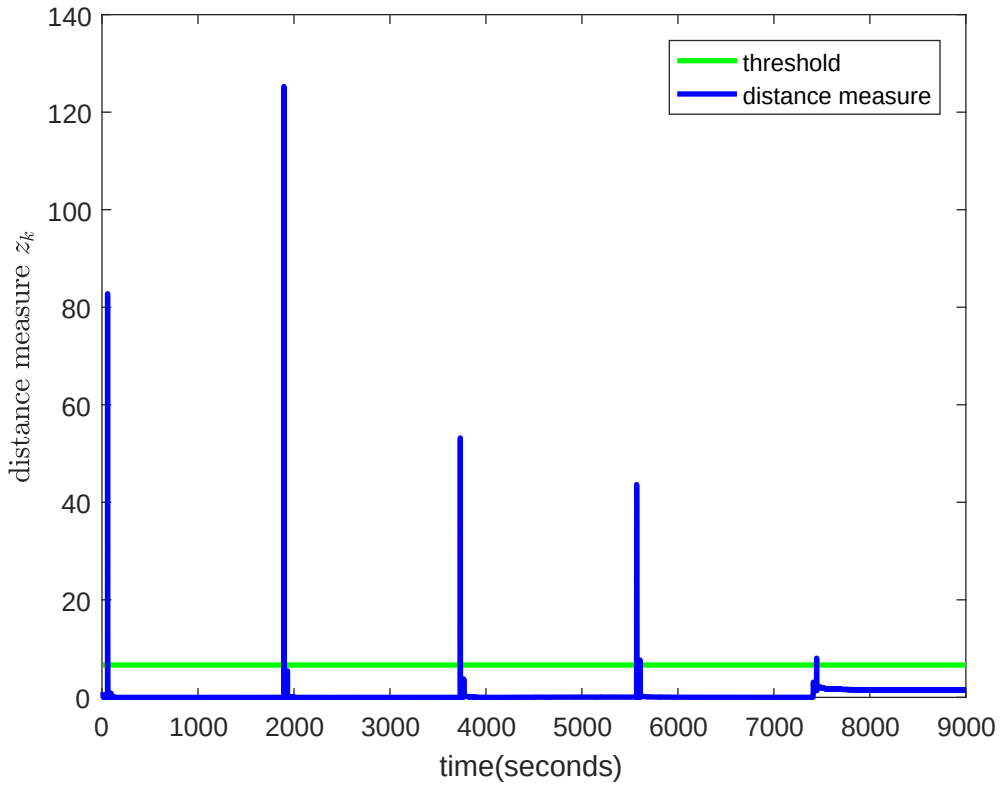

Figure 7.2. Distance measure of the dynamic estimator.

Figure 7.2 illustrates the distance measure plot for an estimator with varying model parameters. Although the distance measure in the rest phase lies below the threshold, the distance measure during the discharge exceeds the threshold. This is because of the sharp transition of parameters during the discharge phase and 10% drop of SOC. Figure 7.3 shows the transition of parameters at the discharge phase.

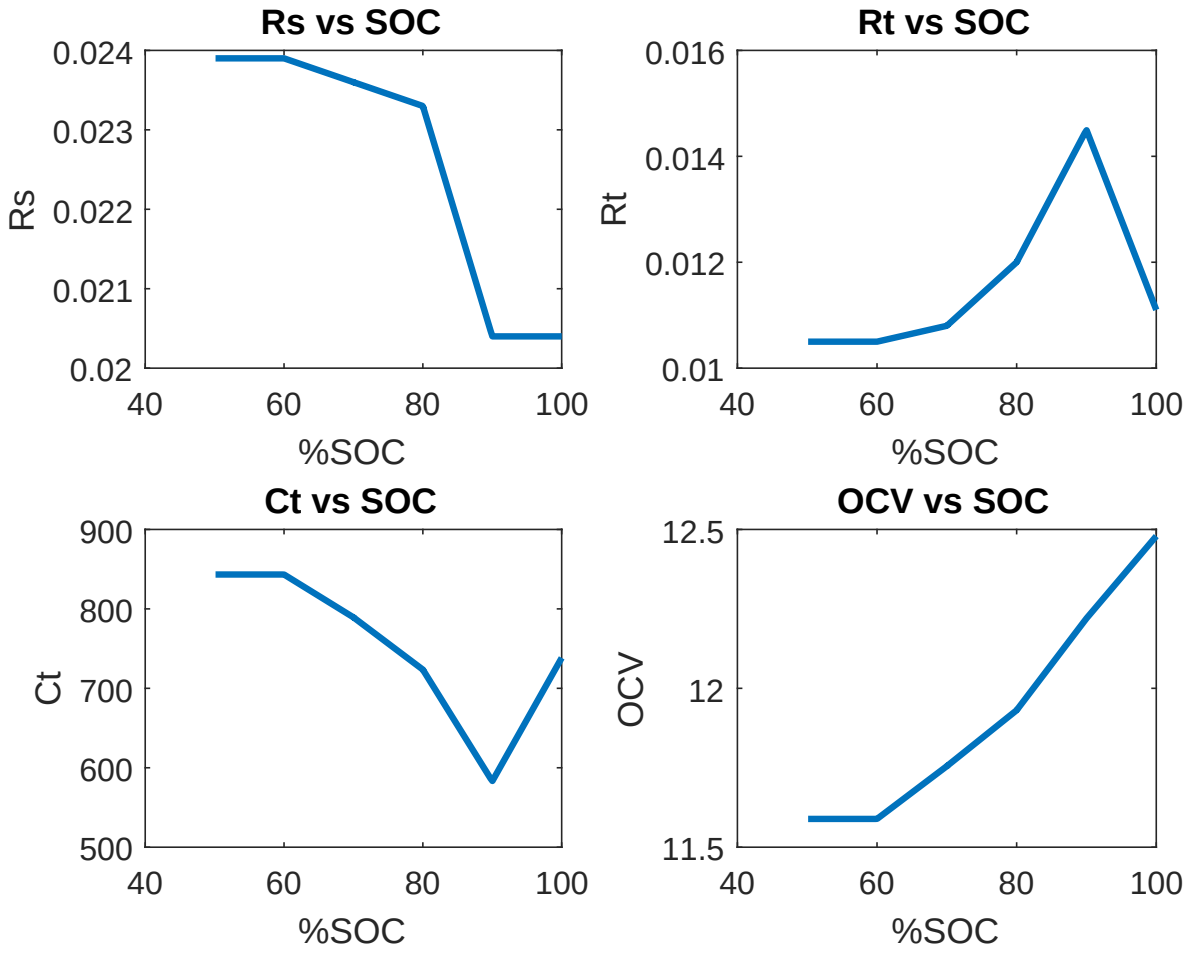

Figure 7.3. Parameter scheduling

To overcome the transitions which cause the distance measure to exceed the threshold, we interpolate the parameter values to obtain a smooth parametrization of available data so that results at intermediate (or extended) positions can be evaluated. This is similar to synthesizing data during the discharge phase to obtain smoother transitions. Figure 7.3 represents the interpolated model parameters at different SOC values. The SOC is calculated using coulomb counting and the model parameters are interpolated with the SOC at each time step to obtain more samples between the transitions. Using these model parameters,

the system and the Kalman filter is updated at each time step, at the corresponding SOC value for detection of anomalies.

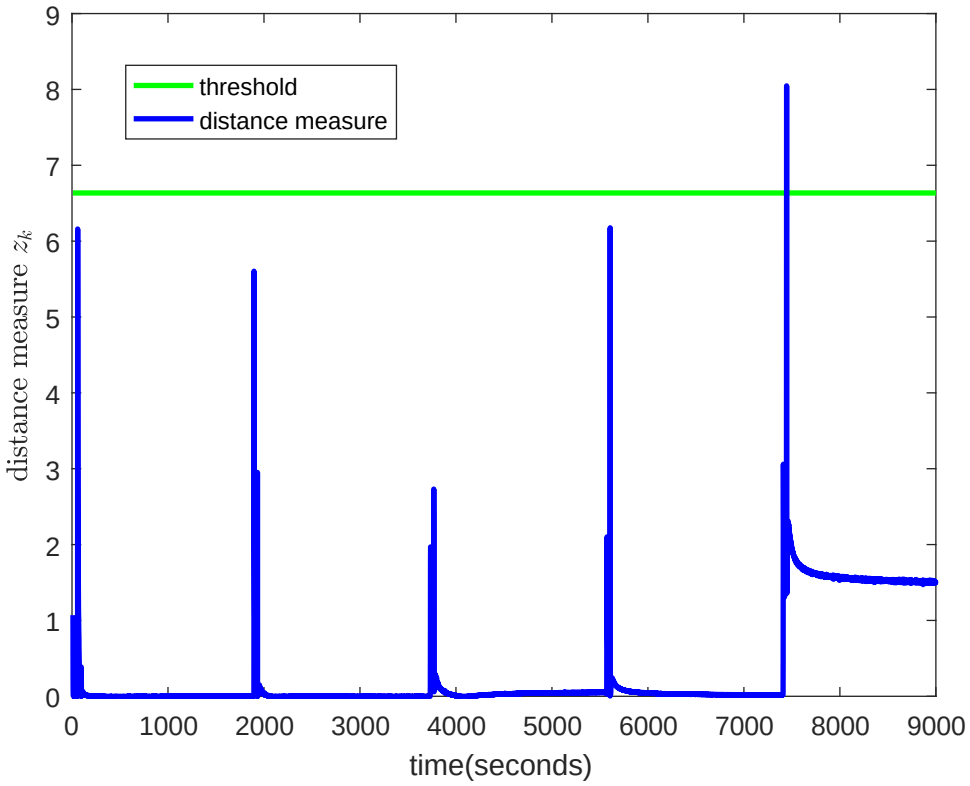

Figure 7.4. Distance measure for interpolated parameter scheduling.

In Figure 7.4 we can observe that after interpolation, the distance measure lies below the threshold, and performs better detection operation.

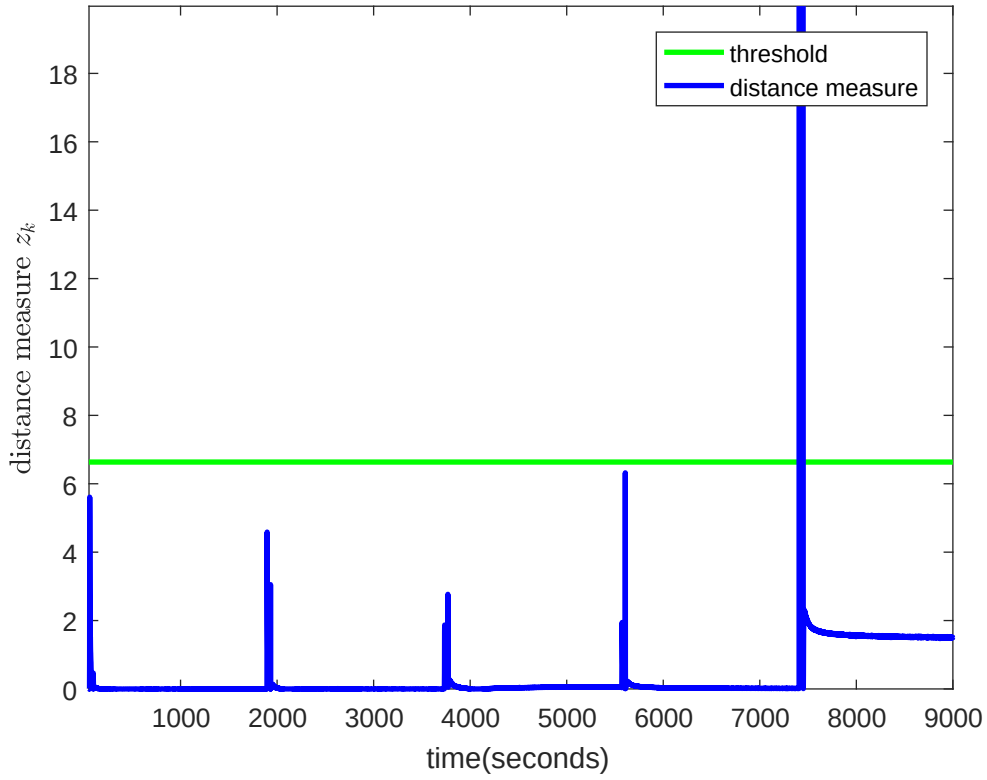

Figure 7.5. Distance measure for interpolated parameter scheduling for an induced failure in the battery

Figure 7.5 illustrates the detection of an anomaly using the data where a fault/failure was induced during a discharge phase. This could also be termed as an attack in this case. An example of an attack in the battery can be spoofing or modifying the sensor measurements. Here the measured output voltage was modified (zeroed out the terminal voltage) during the last discharge phase i.e. approximately for 30 seconds. So, the distance measure blows up to a very high value (in the order of 10^5) indicating an anomaly.

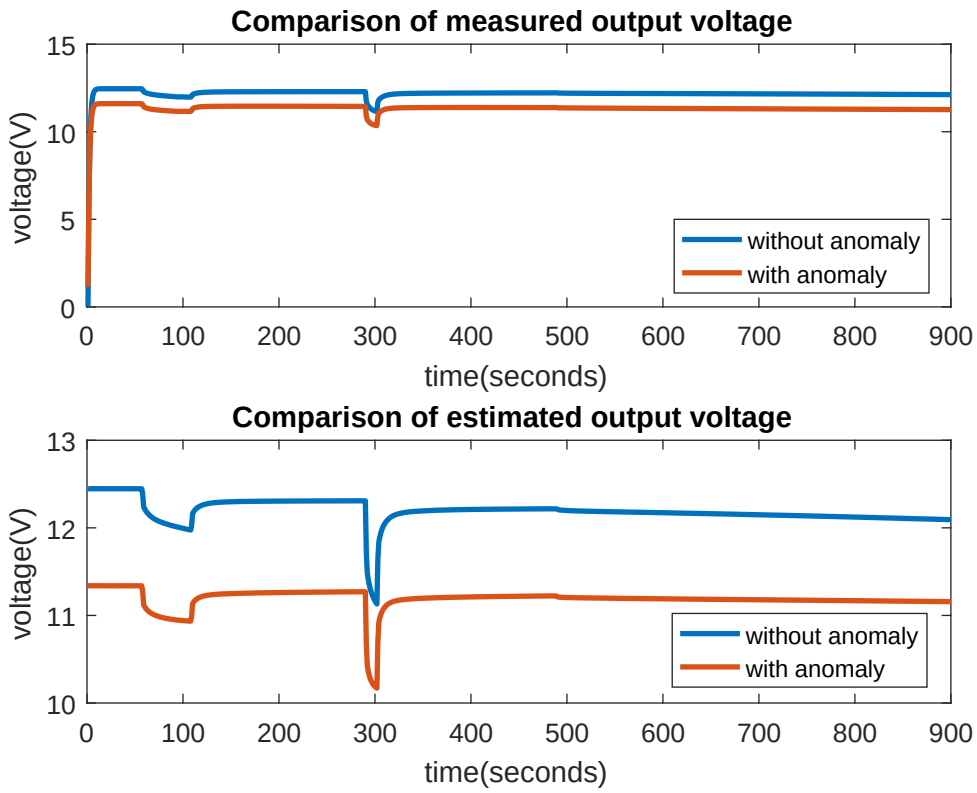

Figure 7.6. Comparison of performance for a properly functioning battery and for a battery with an anomaly of low magnitude

Figure 7.6 shows the comparison of output voltage and estimated voltage for a properly functioning battery and for a battery with an anomaly. The voltage difference being very small, it indicates an anomaly of low amplitude. Drive cycle test is performed on two batteries of the same kind and one of the batteries indicated improper functioning which was later understood to be the cause of a calibration error in the cycling station. This can also be an example of an anomaly and particularly the one with a low amplitude. The first plot illustrates the comparison of the measured terminal voltage of the two batteries. The battery with an anomaly does not perform as expected and shows a deviation in the output voltage. The second plot indicates the output voltage as estimated by the Kalman filter for the same two batteries. For the battery with an anomaly the measured output voltage

deviates from the estimated output voltage for a battery without an anomaly. Using the measured and the estimated terminal voltages the distance measure is determined and is plotted as shown below.

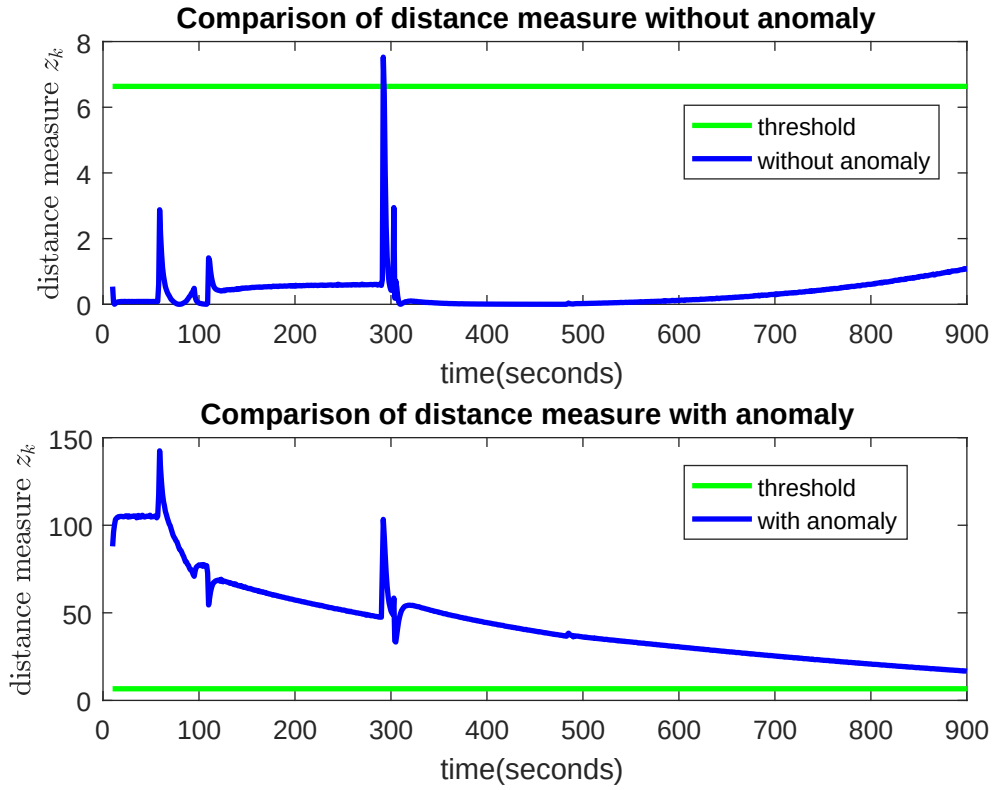

Figure 7.7. Distance measure for interpolated parameter scheduling for a battery failure.

Figure 7.7 shows the detection of an anomaly in battery tested data with a calibration error in the cycling station. For the drive cycle test performed on the battery, the estimation error is very high. The estimated voltage is deviated from the measured terminal voltage causing the distance measure to exceed the threshold at each time step indicating an anomaly in the battery. The first plot indicates the distance measure for a battery under good condition where the distance measure lies below the threshold. The second plot shows distance measure plot for the battery with an anomaly where the distance measure exceeds the threshold indicating the improper behavior of the battery.

CHAPTER 8

CONCLUSION AND FUTURE WORK

8.1 Conclusion

In this thesis, we implemented a residual based detection mechanism for anomaly detection in batteries. We used a Kalman filter to estimate the output voltage of a Li-ion battery modeled into a first order RC equivalent circuit and demonstrated the implementation of an adaptive estimation algorithm based on least squares technique for on-board estimation of model parameters. We studied the working of various detectors. We explicitly analyzed the performance of windowed chi-squared detector to understand the trade-offs between false alarm rates and window lengths. In this research, we focus on stealthy attacks and tune the detectors for worst-case attack detection.

8.2 Future Work

In this thesis we consider the modeling of Li-ion into a simple Randle's circuit which is a first order RC equivalent circuit. This does not consider the hysteresis voltage. Ignoring this voltage in estimation could lead to large errors. By implementing an enhanced model of the Li-ion battery, we can consider the hysteresis voltage. For further improvement, an enhanced self-correcting model can be considered. This model considers OCV and the hysteresis during rest, and considers OCV, hysteresis and the voltage drops across the resistors during constant current event. This helps in obtaining a very accurate estimate. In addition to this, it is important to consider the implementation of an extended Kalman filter to account for the non-linear dependency of the model parameters on the state of charge. Implementation of an extended Kalman filter (EKF) on an enhanced self-correcting model (ESC) gives accurate state estimates.

REFERENCES

(2008, December). Guide to understanding battery specifications. http://web.mit.edu/evt/summary_battery_specifications.pdf.

Battery University (2016). Battery university. http://batteryuniversity.com/learn/article/lithium_based_batteries.

Chaoui, H. and S. Mandalapu (2017). Comparative study of online open circuit voltage estimation techniques for state of charge estimation of lithium-ion batteries. *Batteries 3*(2), 12.

Chiang, Y.-H., W.-Y. Sean, and J.-C. Ke (2011). Online estimation of internal resistance and open-circuit voltage of lithium-ion batteries in electric vehicles. *Journal of Power Sources 196*(8), 3921–3932.

Dong, G., X. Zhang, C. Zhang, and Z. Chen (2015). A method for state of energy estimation of lithium-ion batteries based on neural network model. *Energy 90*, 879–888.

G.L.Plett (Autumn 2015b). Lecture notes on modeling, simulation, and identification of battery dynamics. http://mocha-java.uccs.edu/ECE5710/index.html.

G.L.Plett (Spring 2015a). Lecture notes on battery management and control. http://mocha-java.uccs.edu/ECE5720/index.html.

Hu, R. (2011). Battery management systems for electric vehicle applications. https://scholar.uwindsor.ca/cgi/viewcontent.cgi?article=6006&context=etd.

Kepco Inc. (2012). Operator's manual. http://www.kepcopower.com/support/2431295-r4b.pdf.

Lancaster, H. (November 1969). *The chi-squared distribution*. Wiley series in probability and mathematical statistics. Probability and mathematical statistics.

Liu, C., Z. G. Neale, and G. Cao (2016). Understanding electrochemical potentials of cathode materials in rechargeable batteries. *Materials Today 19*(2), 109–123.

Murguia, C. and J. Ruths (2016a). Characterization of a cusum model-based sensor attack detector. In *Decision and Control (CDC), 2016 IEEE 55th Conference on*, pp. 1303–1309. IEEE.

Murguia, C. and J. Ruths (2016b). Cusum and chi-squared attack detection of compromised sensors. In *Control Applications (CCA), 2016 IEEE Conference on*, pp. 474–480. IEEE.

Murnane, M. and A. Ghazel (2017). A closer look at state of charge (soc) and state of health (soh) estimation techniques for batteries.

Qadeer, R., C. Murguia, C. M. Ahmed, and J. Ruths (2017). Multistage downstream attack detection in a cyber physical system. In *Computer Security*, pp. 177–185. Springer.

Tunga, Murguia, C. and R. Justin (2018). Tuning windowed chi-squared detectors for sensor attacks. In *American Control Conference (ACC), 2018 IEEE Conference on*, pp. to appear. IEEE.

Turnigy (2018). Turnigy power systems. `http://www.turnigy.com/`. Battery Specs.

USB-6008 (2018). National instruments. `http://www.ni.com/en-us/support/model.usb-6008.html`. website.

Weicker, P. (31 Jan 2014). *A Systems Approach to Lithium-Ion Battery Management*. Norwood, USA: Artech House Power Engineering.

Xiong, R., L. Lv, and H. Mu (2017). A novel grouping method for lithium-ion battery pack considering cell divergence. In *Chinese Automation Congress (CAC), 2017*, pp. 5269–5273. IEEE.

BIOGRAPHICAL SKETCH

Tunga R was born in Bangalore, Karnataka, India. She received her Bachelor of Engineering from BNM Institute of Technology affiliated to Visveswarya Technological University (VTU) in Electronics and Communication in June 2016. Later, she joined The University of Texas at Dallas, Richardson, TX, USA in Fall 2016 for Master of Science in Electrical Engineering. She worked under Dr. Justin Ruths during the course of her master's degree. Her research interests include Battery Controls, Battery Management Systems (BMS), Kalman filters, Anomaly Detection, State of Charge estimation of Li-ion batteries.

Tunga Rangaswamy

Dallas, Texas
United States
✉ *txr160830@utdallas.edu*

"Work until you no longer have to introduce yourself!"

Education

2016 - 2018 **University of Texas at Dallas - M.S. in Electrical Engineering**, *CGPA - 3.376/4.0.*
Area of Concentration: Dynamic Systems and Control

2012 - 2016 **Visvesvaraya Technological University - B.E. in Electronics Engineering**, *CGPA - 3.6/4.0.*

Research: *Graduate Student Researcher*

Sept 2017 - Present **Fault Detection in Battery Packs**.

- State of Charge (SOC) and State of Health (SOH) estimation of the battery
- Developing algorithms for state and parameter estimation of Li-ion battery models
- Implemented a model-based approach to detect the failures and attacks in the Li-ion batteries
- Implemented an adaptive estimation algorithm based on least squares technique to estimate system (Li-ion battery) parameters
- Application of Kalman Filters and Extended Kalman Filters for Battery Management Systems

Jun 2017 - Aug 2017 **Tuning Windowed Chi-Squared Detectors for Sensor Attacks**.

- Proposed model-based windowed chi-squared procedure for identifying faulty/falsified sensor measurements
- Static chi-squared and the cumulative sum (CUSUM) fault/attack detection procedures were used as benchmarks to compare the performance of the windowed chi-squared detector
- Characterized the state degradation that a class of attacks can induce to the system while enforcing that the detectors do not raise alarms (zero-alarm attacks)
- Quantified the advantage of using dynamic detectors (windowed chi-squared and CUSUM detectors), which leverages the history of the state, over a static detector (chi-squared) which uses a single measurement at a time
- Simulations using a chemical reactor were presented to illustrate the performance of our tools

Professional Experience

Oct 2017 - Present **University of Texas at Dallas**, *Grader and Teaching Aide: Systems and Controls*.

- Evaluated the performance of the students and their understanding of the classical control theory and control laws
- Guided students to derive and analyze dynamic models of mechanical, electrical, and electromechanical systems using time and frequency-domain representations, and to analyze the stability and performance of control systems in time and frequency-domain
- Assisted in designing control laws based on time-domain and frequency-domain specifications using Root Locus and Bode Plot methods

Oct 2017 - Dec 2017 **University of Texas at Dallas**, *Lab Assistant: Circuits and Applied Electronics*.

- Instructed and trained students in understanding and conducting experiments with circuit components (resistors, capacitors, inductors, component networks), power concepts (AC, DC, single and 3-phase), basic microelectronics (semiconductors, diodes, transistors, op-amps, amplifiers), and digital design (number systems, logic circuits, common ICs).

Jan 2016 - Jun 2016 **National Aerospace Laboratories (CSIR-NAL)**, *Research Assistant*.

- Designed, tuned and analyzed PID controllers to obtain the desired signal specifications
- Analyzed trajectory planning of Autopilot systems that utilized PID control

Jan 2015 - Feb 2015 **TATA POWER SED**, *Microcontroller Based Systems Intern*.

- Analyzed the design and performance of the: Trusted Desktop Platforms-2 Mother Board Assembly, LPC408x/7x ARM Cortex-M4 based Digital Signal Controller, Fan Controller PCB
- Visited the: Module Bay-Assembly, Clean Room, Testing Department (tested Jig for Serial I/O Isolation Assembly), System Integration Department (tested set-up for RE101 audio analog delay effects unit), EMI/MC Department (tested the emission and susceptance of the modules and its integration), Environmental Testing Lab (conducted PREET and POET tests)

Academic Projects

Aug 2017 - Dec 2017 **Optimization of PID Controller for an Internal Combustion Engine**.

- Optimized the gains of a tuned PID Controller to maintain the engine speed at a prescribed set-point by actuating the electronic throttle
- Implemented Genetic Algorithm and FMINCON optimization routines to make the PID Controller robust to tune itself for different control applications
- Investigated the performance of the tuned PID Controller for different objective functions, initial conditions and bounds
- Genetic Algorithm provided better optimization compared to Ziegler-Nichols tuning and FMINCON optimization routine
- FMINCON yielded satisfactory response with very less time as compared to the Genetic algorithm.

Jan 2017 - May 2017 **Idle Speed Control and Air-fuel ratio Control of an Internal Combustion Engine**.

- Built a Simulink model of a 4-cylinder 2.4 L engine to model a plant in discrete domain - Optimized the throttle angle to maintain an idle speed of 800 rpm using a SISO controller
- Developed and tuned a PID controller for the idle speed control and achieved zero steady state error
- Utilized Root Locus techniques to develop a controller to compare with the results of PID control
- Developed a MIMO controller to maintain the air-fuel ratio

Aug 2016 - Dec 2016 **Detecting Speech Activity using Convolutional Neural Network Classifier**.

- Created a low memory (Parameter Memory 676 KB and Data Memory 49 MB) and a computationally efficient (Processing Time: 30 seconds) Convolutional Neural Network (CNN)
- Extracted the data set from the features which are in the form of images stacked as vectors. The data set consisted of 3 folders: SNR-0, SNR-5 and SNR-10 where each folder contains the MEL-frequency spectral coefficient features
- Each image archive consisted of files in 5 batches where each batch remained independent of other to allow cross validation
- Generated Confusion matrix by averaging the cross-validation analysis
- Utilized 3 batches of data for Training, one for Testing and the remaining one for Validation
- Trained, Tested and Analyzed CNN classifier architectures by using MatConvNet open-source library
- Developed a 91% accurate CNN classifier to separate speech and non-speech (noise) segments of audio files which use Mel-frequency spectral coefficients as input features (Deep Learning)

Jan 2016 - May 2016 **WLAN Frame Classification to Access Category Based on User Priority**.

- Inserted Priority value- Priority Code Point (PCP) in Ethernet frame by VLAN (Virtual Local Area Network) tagging
- Extracted PCP bits from the Ethernet frame and mapped to corresponding Access categories where the contention for the channel is differential, based on user priority
- Enhanced Distributed Channel Access (EDCA) method was used to support Quality of Service (QoS) requirements where priority is based on 802.1e and is determined using various parameters: maximum and minimum contention window, Arbitrary Inter-frame Spacing (AIFS), Transmission Opportunity (TxOP)

Jan 2014 - Jul 2014 **Low Cost ECG Device and Heart Rate Monitor** .

- Designed a reliable integrated device which can display an ECG signal and monitor the heart beat
- Implemented using basic analog components
- Utilized Instrumentation amplifier and filter circuits for signal conditioning
- Soldered the circuit design on PCB

Systems and Control Proficiencies

Modeling: Automotive Powertrain Systems

Control: Kalman Filter, State Feedback, LQR, Lyapunov Redesign, Feedback Linearization, Input-Output Linearization, Integrator Backstepping, Passivity Based Control, Adaptive Control, Force Control, PID Control, Optimization Theory, Root Locus Design, Bode and Nyquist Plots

Tools

Controls: Matlab/ Simulink, Python, C, C++

Electrical: Visual Studio, ISE simulator: Xilinx Cadence, PCB Design

Computer: MS Office

Graduate Coursework

Linear Systems	Modeling and Simulation
Nonlinear Systems	Pattern Recognition
Digital Control of Automotive Powertrain	Random Processes
Robust Control	Optimization Theory and Practice

Undergraduate Coursework

Control Systems	Computer Aided Drawing
Elements of Mechanical Engineering	Network Analysis
Signals and Systems	Digital Signal Processing
Power Electronics	DSP Algorithms and Architecture
Embedded System Design	Image Processing
Real Time Operating Systems	Microcontrollers and Microprocessors

Publication

2015 **"Gesture Controlled Musical Instrument" at IEEE IC-SSS-2015 International Conference, published in IEEE Xplore (elaborate)**.

Abstract: This paper explores the feasibility of a musical instrument incorporating digital signal processing coupled with SONAR to produce musical notes by emulating conventional instruments using cost effective hardware

Proposed signal processing methods tending to emulate the sounds produced in conventional instruments. Explored the feasibility of the proposal by implementation on a cost-effective hardware

Link to the published paper: http://ieeexplore.ieee.org/document/7873597/

Certification

- NIIT Certified course: Programming in C
- NIIT Certified course: Object Oriented Programming in C++
- Matlab-Arduino workshop

Leadership

Dec 2015 - Jun 2016 Chairperson of the IEEE-BNMIT student branch

Activities

- Organized various technical and non-technical events at the inter-college level
- Participated in IEEE Student Leadership Congress-2015
- Volunteered for the IEEE SmartTech workshop-2015
- Volunteered for the India Electronics Week organized by Electronics for You (EFY) in collaboration with IEEE
- Participated in Texas Instruments Innovation Challenge India Design Contest 2015
- Participated in Texas Instruments India Analog Maker competition